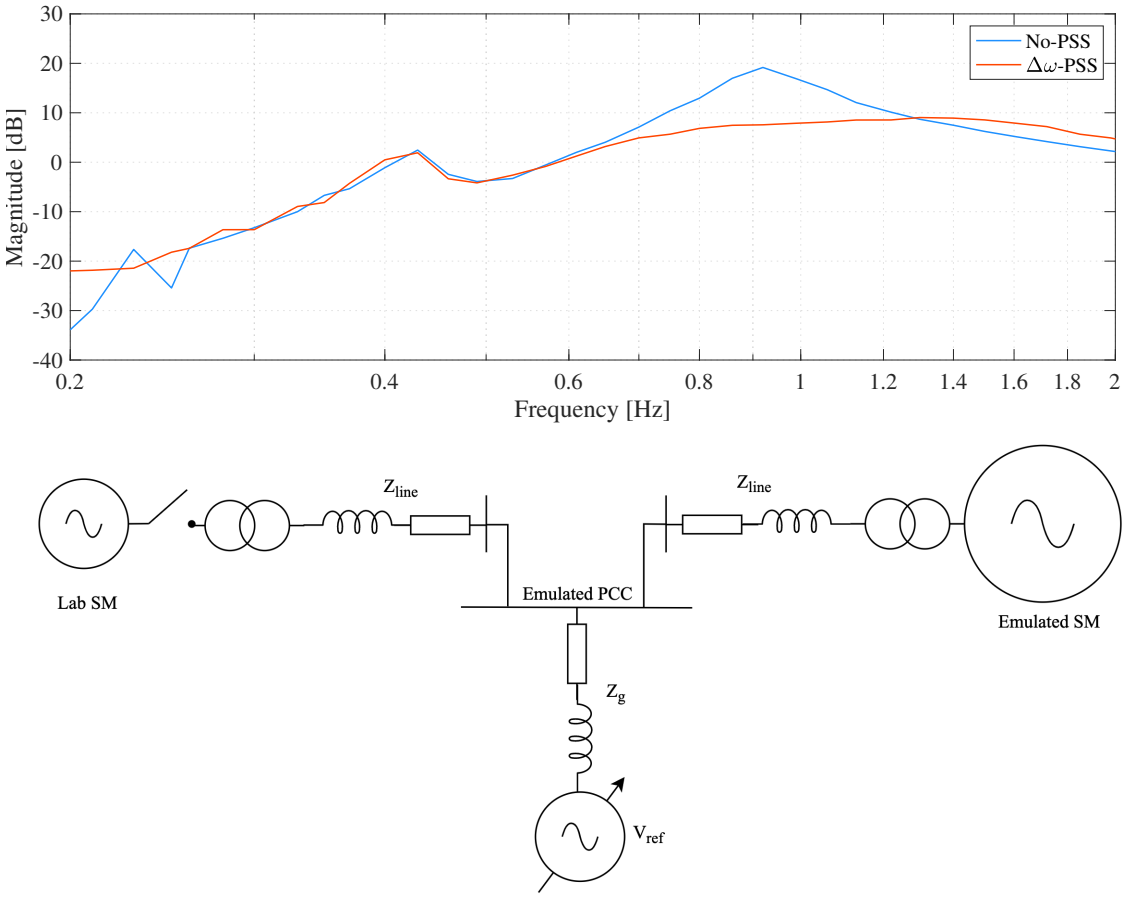

Power Oscillations in Emulated Grid Model

Observing Inter-Area Oscillations in a Power Hardware-in-the-Loop Setup

Master's thesis in Electric Power Engineering

CHRISTIAN EKSTRAND

DEPARTMENT OF ELECTRICAL ENGINEERING

CHALMERS UNIVERSITY OF TECHNOLOGY
Gothenburg, Sweden 2022
www.chalmers.se

Master's thesis 2022

Power Oscillations in Emulated Grid Model

Observing Inter-Area Oscillations in a
Power Hardware-in-the-Loop Setup

CHRISTIAN EKSTRAND

CHALMERS
UNIVERSITY OF TECHNOLOGY

Department of Electrical Engineering
Division of Electric Power Engineering
Chalmers University of Technology
Gothenburg, Sweden 2022

Power Oscillations in Emulated Grid Model
Observing Inter-Area Oscillations in a
Power Hardware-in-the-Loop Setup
CHRISTIAN EKSTRAND

Supervisor: Bengt Johansson, Solvina AB
Examiner: Peiyuan Chen, Department of Electrical Engineering

Master's Thesis 2022
Department of Electrical Engineering
Division of Electric Power Engineering
Chalmers University of Technology
SE-412 96 Gothenburg
Telephone +46 31 772 1000

Cover: Displaying the magnitude of the frequency response presented in a bode plot from Figure 5.3, along with the complete system setup in Figure 4.1.

Typeset in LaTeX
Printed by Chalmers Reproservice
Gothenburg, Sweden 2022

Power Oscillations in Emulated Grid Model
Observing Inter-Area Oscillations in a
Power Hardware-in-the-Loop Setup
CHRISTIAN EKSTRAND
Department of Electrical Engineering
Chalmers University of Technology

Abstract

Power oscillations may arise in the power system following ever-changing grid conditions. The system impact in one grid area may differ from another because of different factors such as grid strength, installed generation capacity, available supplementary control and instantaneous flow of power. Demonstrating how these parameters influence a local power plant is made possible in this thesis work by utilizing a power hardware-in-the-loop (PHIL) system to emulate a fictitious adjacent grid area in a physical lab environment. After constructing the grid model in Simulink, the PHIL system became real-time compatible with the physical synchronous machine (SM) located in the down-scaled power system lab at Chalmers. This enables the possibility to apply disturbances in the emulated grid model to interfere with the physical lab when interconnected, allowing the aforementioned grid characteristics to be changeable in real-time. Slow oscillations following a disturbance from an adjacent grid area, dynamically interacting with another is referred to as an inter-area oscillation. These oscillations were observable from the physical SM's perspective. Then with the addition of a power system stabilizer (PSS), the damping contribution added became distinguishable when the local mode power oscillations were suppressed. Thus, the project's objectives are achieved and the developed models will be utilized for future educational demonstrations and training in PSS tuning.

Keywords: emulated grid model, power hardware-in-the-loop, inter-area oscillation, power system stabilizer, simulink, synchronous machine.

Acknowledgements

First of all, I would like to express enormous gratitude equally split between Bengt Johansson and Peiyuan Chen for making this possible and believing in me. Through your invaluable guidance, patience and highly technical expertise, this project was made possible and has been genuinely fun. I would also like to take the opportunity to thank Sven Granfors and all colleagues at Solvina for giving me a warm welcome from day one. Also, big thanks to Jaidev Oza, assisting with the operation of the synchronous machine in the lab, enabling me to produce the results. Lastly, I would like to show appreciation to all my friends, new and old alike for the support I have received throughout the years.

Christian Ekstrand, Gothenburg, May 2022

List of Acronyms

Below is the list of acronyms that have been used throughout this thesis listed in alphabetical order:

AVR	Automatic Voltage Regulator
d-axis	Direct Axis
PHIL	Power Hardware-in-the-Loop
PCC	Point of Common Coupling
PSS	Power System Stabilizer
SM	Synchronous Machine
q-axis	Quadrature Axis

Contents

1
Introduction

1.1 Background

The conventional synchronous machine (SM) based generation powered by fossil fuels are being replaced by more environmental friendly renewable alternatives. This shift in generation technology give rise to several stability related challenges [1–3]. As discussed in [4], there are multiple grid characteristics potentially missing in a future power system, including faster frequency dynamics because of less rotating system inertia available. Power oscillations could thus become more severe throughout the system following a disturbance and the modes of oscillation could either be local if a generation unit is oscillating at its natural frequency towards the power system or directly against generation units in another grid area. The latter one is referred to as inter-area modes of oscillation and when evaluating small signal stability and the system lacks adequate damping, the system could appear in a state beyond its intended stability region where oscillations proceed indefinitely [5]. One way of counteracting such oscillations is to implement a power system stabilizer (PSS), in addition to the automatic voltage regulator (AVR) connected to the excitation system of a SM [6]. Hence, the voltage at the SM can be regulated to damp out inter-area swings and alleviate power oscillations over certain frequencies [7, 8].

Observing inter-area oscillations in a physical lab environment is made possible using a digital power hardware-in-the-loop (PHIL) system [9], able to replicate a fabricated power grid in real-time. This enables the interconnection between a physical power generation unit and a simulation based system constructed in Simulink, compatible with the PHIL system [10]. Thus, emulating a physical point of common coupling (PCC) with varying grid characteristics, designed to initiate inter-area swings. To obtain further knowledge within the field and facilitate future training in PSS tuning, an emulated grid model is constructed inside the electrical power system lab at Chalmers.

1.2 Aim

The aim of this Master thesis is to design a PHIL system to emulate a fictitious grid area with adjustable system characteristics in a Simulink based control environment. The emulated fictitious grid consists of a Thevenin grid model and a down-scaled power plant model which is connected to a physical SM for studying inter-area power oscillations. The laboratory setup will be used for future educational purposes.

1.3 Task

To successfully demonstrate inter-area oscillations between the physical lab setup and the simulation based power system through a PHIL configuration, a Simulink model is designed accordingly. This is the most essential task, being the backbone of the project when developing an emulated grid area compatible with the PHIL system and lab environment in real-time. By exposing the two grid areas with fabricated perturbations through the emulated model, enables power oscillations to be observed. This is accomplished by constructing a manually operable reference voltage source, governing the set-point for grid forming characteristics, along with an emulated SM model, dynamically initiating inter-area swings. Furthermore, a user friendly interface is constructed to facilitate real-time operation through the PHILs experimental software in the lab environment.

To achieve the right grid conditions for inter-area swings to arise within predetermined frequency spectrum, the two grid areas are reconstructed into a simulation based environment. With the use of Simulink's available software tools, the interconnected power system is linearized to analyze the dynamic frequency response, which is observed in bode diagrams. The grid parameters impacting the modes of oscillations are examined and the mitigating action provided by installing a PSS is noted. Lastly, these aforementioned tasks are reiterated and demonstrated in the physical lab environment to evaluate the emulated grid models functionalities, along with the inter-area interaction when implementing the PSS to the physical SM.

1.4 Scope

The scope of this study come with the following delimitations to facilitate the methodology of achieving the projects objective:

- The functionality of the PSS along with its oscillatory damping properties is implemented for illustrative purposes only, using a simplified model. Thus, no additional analyses are performed to tune the PSS parameters to achieve optimal damping effects. Similar approach is considered when implementing the AVR to the emulated SM to obtain a realistic system response.
- The emulated SM model used consists of a pre-built Simulink block, modelling the electrical and mechanical dynamics instead of manually constructing it. This makes it possible to vary grid parameters and to redirect power flow within the emulated grid model.
- The bode diagrams and system responses presented is mainly focusing on the the power amplification response when analyzing the results. This is to delimit the study and clearly illustrate how certain grid conditions and parameters impact power oscillations.

1.5 Sustainability Aspects and Ethical Dilemmas

Some reflections related to this thesis work regarding social, environmental and ethical effects are discussed here. An interconnected power system should maintain stability and thus supply reliability while continuously supplying customers, regardless of these aforementioned aspects. Still in some areas on this planet, this necessity is not guaranteed. United Nations sustainable development goal number 7 of the 2030 agenda, set back in 2015, states [11]:

"Ensure access to affordable, reliable, sustainable and modern energy for all".

The IEA energy progress report [12], tracks the forgoing sustainable development goal and forecasts an steady increase in the renewable energy base decentralized solutions. The challenges are discussed especially in market structure and value chains for the individual actors involved to achieve this goal while maintaining power system stability. This approach sees to focus on less conventional SM based generation, especially in densely populated areas. However, insufficient mitigating damping control is available in interconnected grids with high renewable energy penetration. The system is intentionally underdimensioned for achieving cost-effective solutions. However, this may result in similar phenomenons being brought up later in this project. When power oscillations arise without mitigating action available, wear and tear or disrupted power supply may be experienced in adjacent grid areas. The reduced system damping will result in inter-area oscillations that may worsen the conditions for neighboring grid operators, consequently slowing down development in case of an interruption in power supply.

1.6 Outline

The outline of the thesis report is structured as follows:

Chapter 1:
Introducing the background description and objectives of the thesis work.

Chapter 2:
Introduction of fundamental theory, with special emphasis on power system stability.

Chapter 3:
Introducing the real-time interface architecture of the PHIL system, along with practical implementation in Simulink.

Chapter 4:
Evaluating system study and grid characteristics impacting modes of oscillation through simulations before physical lab results.

Chapter 5:
Presentation of physical lab test results.

Chapter 6:
Lastly, conclusions are drawn, including recommendations for future work.

2

Power System Stability

This chapter introduces the fundamental aspects regarding stability in an ever-changing dynamic interconnected power system. The generator rotor angle stability refers to the maintainance and restoration of the equilibrium between electrical and mechanical torque following a perturbation, without jeopardizing the operation as a whole [13]. To get acquainted with the electromagnetical oscillations, the essential characteristics of the SM will first be introduced, followed by the description of common supplementary control techniques enhancing system stability.

2.1 Synchronous Machine Fundamentals

The conventional three-phase SM constitutes of two main magnetic parts, the cross section illustrated down in Figure 2.1, showing the inner stator surface where the armature winding for each current conducting phase is situated. Whereas the field winding, carrying the dc current and producing a rotating magnetic field, inducing each armature phase voltage is placed on the rotor. Each stationary armature phase winding arrangement is displaced 120° uniformly apart to produce a magnetic field in the air-gap that is rotating at synchronous speed [6]. The field winding magnetic flux is aligned with the rotors direct axis (d-axis), while the quadrature axis (q-axis) is leading the d-axis by $\pi/2$ electrical radians ahead, where the induced electromotive force is referenced.

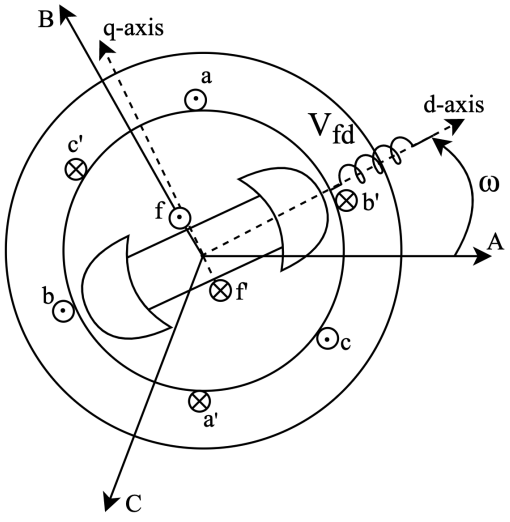

Figure 2.1: Overview of the winding arrangement and axis alignment in a salient-pole SM.

Thus, the rotor angular velocity yields the instantaneous position of the rotor d-axis with respect to the stationary reference frame. The number of field poles determines the mechanical speed of the rotor and electrical angular frequency of the stator currents to produce electromagnetic torque. For salient-pole machines, like the one illustrated in Figure 2.1 has a nonuniform varying air-gap flux in d, and q-direction since the distance to the inner surface of the stator differs over an electrical period.

Salient-pole SMs are regularly used for hydroelectric applications to operate at lower rotational speeds since they cannot withstand such high centrifugal forces as uniformly shaped round-rotor machines used for high speed turbines [14]. Consequently, more field pole pairs results in a slower rotational synchronous electrical speed of 50 Hz. This rotational speed Ω_n, given in rpm in relation to rated system frequency f is defined as,

$$\Omega_n = \frac{120f}{2n_p} \tag{2.1}$$

where n_p is the number of magnetic pole pairs for each phase in the stator slots. Hence, according to (2.1), a salient-pole machine with 3 pole pairs rotates with synchronous speed of 1000 rpm at rated system frequency.

2.1.1 The Swing Equation Dynamics

To further focus on the SM dynamic relationship between electromechanical imbalance and angular deviations, the swing equation is introduced. Starting off with

$$J\frac{d\omega}{dt} = T_m - T_e - K_D\Delta\omega \tag{2.2}$$

describing the angular rotational speed ω in rad/s over a rotating mass with the moment of inertia J in kg$\cdot$ m^2. T_m and T_e are the mechanical and electrical torque respectively in Nm. Additionally, a damping coefficient K_D is considered, including friction and losses and $\Delta\omega$ being the speed deviation.

Furthermore, the inertia constant H describes the amount of seconds the SM can supply nominal rated power S_n from the stored kinetic energy at rated speed ω_n in rad/s. By solving for J

$$H = \frac{1}{2}\frac{J\omega_n^2}{S_n} \Leftrightarrow J = \frac{2H}{\omega_n^2}S_n \tag{2.3}$$

and substituting it back into (2.2) while considering the torque base being defined as $T_{base} = S_n/w_n$ then yields

$$2H\frac{d\omega}{dt} = T_m - T_e - K_D\Delta\omega \tag{2.4}$$

expressed in p.u. for given system base. Given that, the rotor angular position is defined as $\delta = \omega t - \omega_n t$, with respect to synchronously rotating reference, expressed as its time derivative

$$\frac{d\delta}{dt} = \omega - \omega_n = \Delta\omega \tag{2.5}$$

is equivalent to the speed deviation for a small change. Furthermore, the angular acceleration

$$\frac{d^2\delta}{dt^2} = \frac{d}{dt}(\Delta\omega) = \omega_n \frac{d\omega}{dt} \tag{2.6}$$

is the second time derivative of (2.5). During a small perturbation, the speed deviation is much lesser in comparison to the rated synchronous speed ω_n, thus being practically equal to its nominal speed of 1 p.u. [6]. Since the torque in p.u. then is equal to the power in p.u.,

$$\frac{d^2\delta}{dt^2} = \frac{1}{2H}(P_m - P_e - K_D \frac{d\delta}{dt}) \tag{2.7}$$

then finalized the expression of the swing equation above in (2.7). These sets of parameters in the equation can be used to analyze small disturbances around a equilibrium point of operation. The non-linearity of the electrical power P_e will be further elaborated in the upcoming section.

2.2 Small Signal Stability

The electrical power transmitted between two nodes, as seen in Figure 2.2 with an equivalent reactance $X_{eq} = (X'_d + X_g)$ is strongly coupled with the rotor angle [15]. By assuming a lossless condition, the air gap power is equal to the active power,

$$P_e = \frac{E'V_g}{X_{eq}} \sin\delta \tag{2.8}$$

where the internal voltage E' is represented behind X'_d with the rotor angle δ that leads the infinite grid V_g with grid reactance X_g.

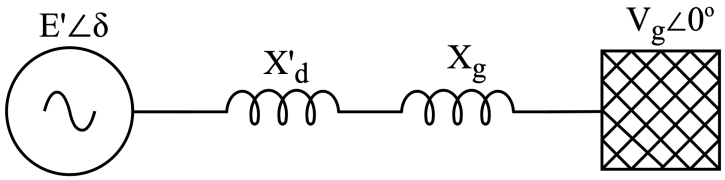

Figure 2.2: SM connected to a strong infinite grid.

The non-linearity of the swing equation back in (2.7) originates from trigonometric part in (2.8), where the electrical power varies with respect to δ. The output power rises by further increasing the rotor angle up until its maximum value

$$P_{e,max} = \frac{E'V_g}{X_{eq}} \tag{2.9}$$

occurring at 90° as illustrated below in Figure 2.3. There, the mechanical power P_m is assumed to be constant and the two lines shown demonstrates how the electrical

power varies as a function of δ if there is a disturbance in any of the parameters in (2.9) following a temporary fault.

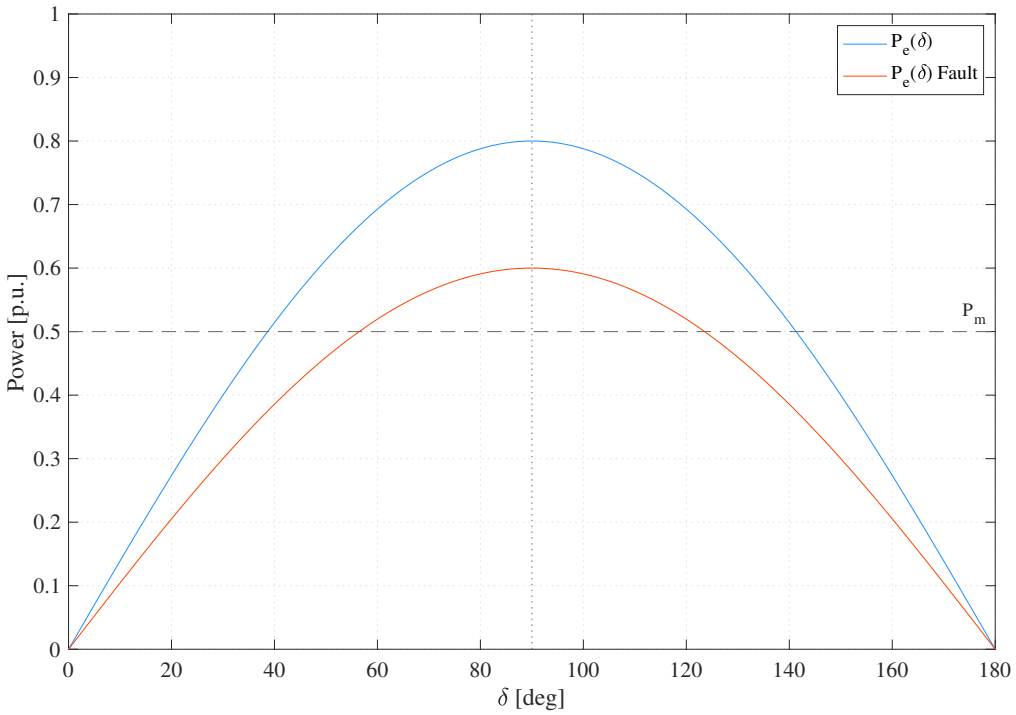

Figure 2.3: Power-angle curves with varying electrical output.

During a smaller disturbance or larger transient, there might be a drop in P_e, causing an imbalance in (2.7). If the net mechanical torque acting on the SM's shaft is greater than the electrical output, the machine will accelerate, and vice versa, the machine starts deaccelerating if the mechanical torque is lesser. Consequently, the imbalance acting on the rotating inertia causes the power to swing back and fourth [16]. Without the damping torque coefficient K_D introduced in (2.2) proportional to the speed deviation, the oscillations could theoretically proceed indefinitely.

Moreover, the initial power swing should not surpass a critical angle that could jeopardize the SM falling out of synchronism from the imbalance caused by the contingency [14]. By applying linearization around the systems operation point, the impact of small displacements in the rotor angle $\Delta\delta$ are practically deemed identical to the initial angle and thus, enabling the non-linear systems stability to be analyzed around steady-state. The synchronizing power coefficient K_S describing the systems ability to mitigate power swings and is defined as

$$K_S = \frac{d}{d\delta}(P_{e,max}\sin\delta) = P_{e,max}\cos\delta \tag{2.10}$$

obtained by substituting (2.9) into (2.8). Consequently, increased synchronizing power is obtained when operating at lower rotor angle, at higher generator terminal voltage as well as in stronger grids [6]. Furthermore, by substituting (2.10) into

(2.7), the linearized version swing equation in p.u.

$$\frac{d^2\Delta\delta}{dt^2} = \frac{1}{2H}(\Delta P_m - K_S\Delta\delta - K_D\frac{d\Delta\delta}{dt}) \tag{2.11}$$

is finally realized. The system input-output dynamics can be expressed in state-space form $\dot{\mathbf{x}} = \mathbf{Ax} + \mathbf{bu}$ [17], to highlight which system state is coupled with the coefficient for damping and synchronizing power. The state variables together with the system matrix result in a system response

$$\frac{d}{dt}\begin{bmatrix}\Delta\omega \\ \Delta\delta\end{bmatrix} = \begin{bmatrix}\frac{-K_D}{2H} & \frac{-K_S}{2H} \\ 1 & 0\end{bmatrix}\begin{bmatrix}\Delta\omega \\ \Delta\delta\end{bmatrix} + \begin{bmatrix}\frac{1}{2H} \\ 0\end{bmatrix}\Delta P_m \tag{2.12}$$

from the added mechanical system input, this state-space representation is observed in Figure 2.4 when there is a small power imbalance.

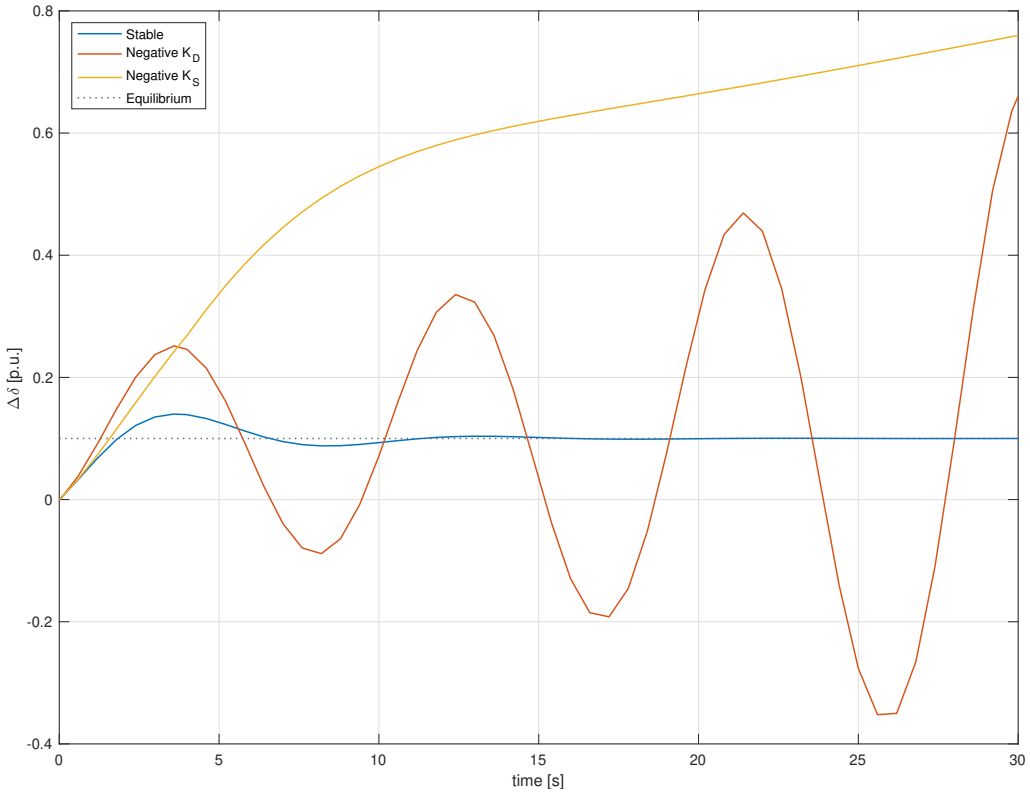

Figure 2.4: Rotor angle influence of K_D and K_S for a small disturbance.

It is seen that when there is insufficient amounts of K_S, the rotor angle deviates rapidly with the disturbance. Similarly, for a poorly damped system with negative a K_D causes the rotor angle to oscillate with ever-increasing amplitude in phase with the speed deviations. To further elaborate on the improvements that can be made on this, the excitation system of the SM will be investigated in the upcoming section.

2.3 Excitation and Automatic Voltage Regulator

In order for the SM to output electrical power to the interconnected grid, there must be an electrical source providing excitation. The purpose of the excitation system, either via static or rotating exciters is to provide a magnetizing field current into the rotor [18]. This in turn enables controllability of the machines terminal voltage to govern the active and reactive power flow within its capability limits. Figure 2.5 illustrates the reactive capability in relation to the electrical output power with the dashed circular shape when considering the SMs physical limitations. Armature and field winding constraints limits the current generated in their windings to avoid too significant thermal strains [6]. Consequently, the SM absorbs reactive power during underexcited operation and injects it to the grid when overexcited.

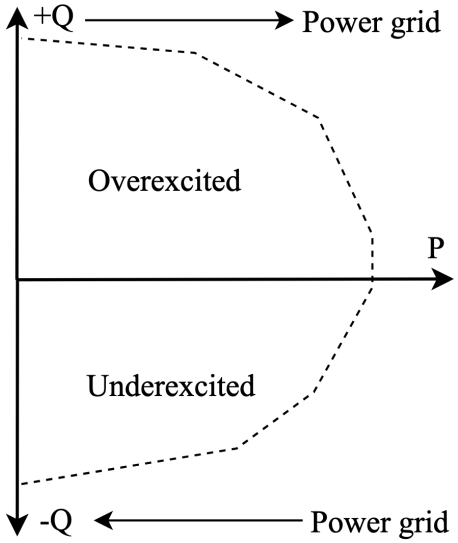

Figure 2.5: Relation between active and reactive power in a SM.

The implementation of an AVR facilitates controllability of the voltage through the excitation system by comparing the terminal voltage V_t with the desired voltage reference V_t^*. The block diagram of the full excitation system is shown in Figure 2.6, illustrating the closed loop feedback system of the terminal voltage sent from the plant model of the SM, back through a filtering voltage transducer $G_{VT}(s)$ that senses and samples the signal [6].

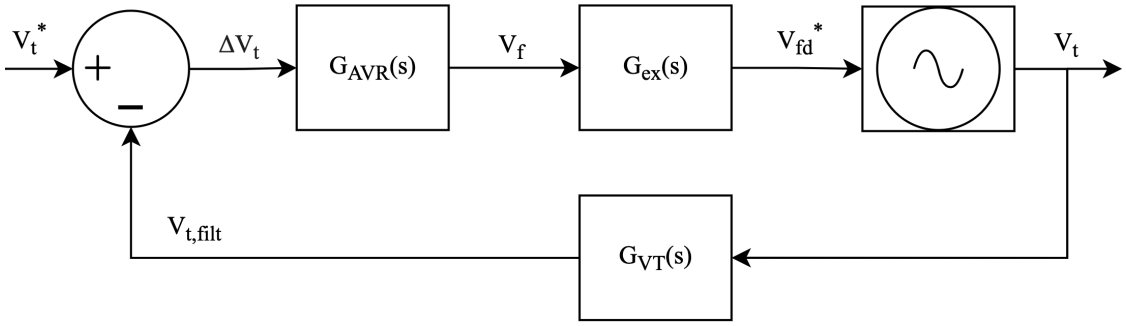

Figure 2.6: Excitation system overview.

One of several available AVR representations is enabled by implementing a PI-regulator as seen in Figure 2.7. It is consisting of a proportional, as well as a integral gain with the objective to push the deviating error towards zero [19].

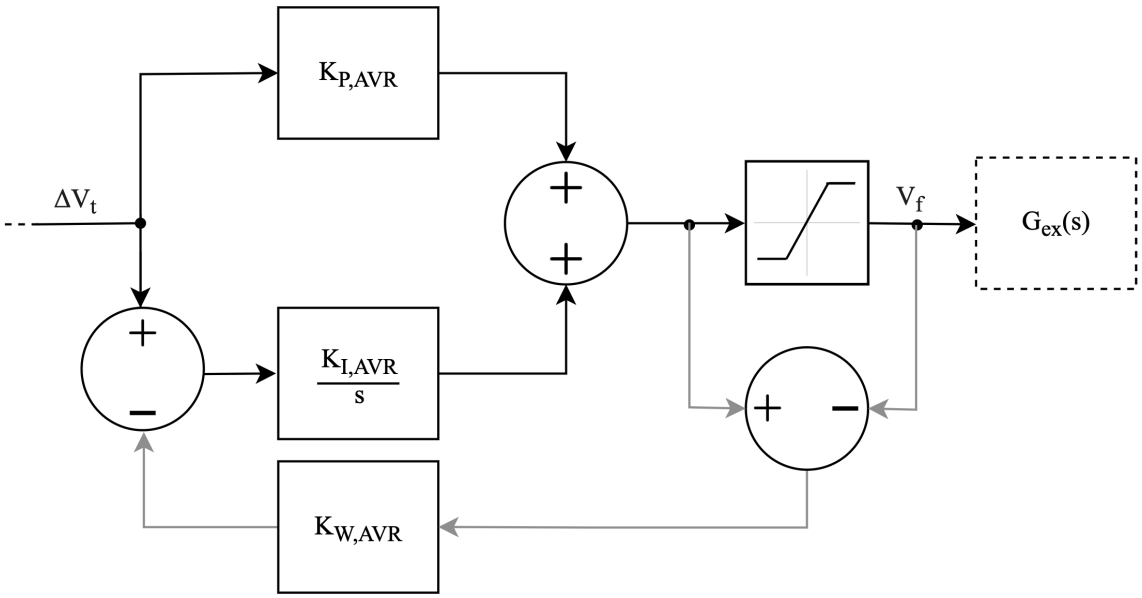

Figure 2.7: Scheme of the AVR implemented with a PI-regulator and anti-windup.

Through negative feedback, the processed voltage deviation ΔV_t is fed to the AVR-block in Figure 2.7 with system gain

$$G_{AVR}(s) = K_{P,AVR} + \frac{K_{I,AVR}}{s} \tag{2.13}$$

when implementing a PI-controller. Additionally, an upper and lower field voltage limiter is set for the regulator before being initialized into the exciter, with the intent to restrain the excitation, considering the aforementioned physical constraints of an SM. If however the limit is reached, the voltage in the regulator becomes saturated and result in a system overshoot. This is due to integrator windup since the PI-controller keep on accumulating a large error between the actual and reference value [17]. The eventual saturated error can be back-calculated and compensated for with an anti-windup gain $K_{W,AVR}$, as seen back in Figure 2.7. Henceforth proving the exciter $G_{ex}(s)$ with given field voltage V_f, letting the excitation system on the SM regulate the terminal voltage following a system disturbance. Moreover, a static exciter can be modelled as a first order low pass filter [15],

$$G_{ex}(s) = \frac{1}{sT_{ex} + 1} \tag{2.14}$$

with a small time constant T_{ex} to obtain a fast system response.

2.4 Power System Stabilizer

The speed deviation dependent component in (2.12), coupled with damping power coefficient K_D may require ancillary service to provide some fine adjustment that the excitation cannot [20]. Even though the AVR alone, can be tuned to mitigate the first swing through the exciter, the fine adjustment provided from the PSS are often needed to damp out electromechanical oscillations in the lower frequency range. As given in [21], classifying the frequency spectrum typically ranging between 0.1-0.7 Hz for inter-area oscillations whereas local ones can propagate up towards 2 Hz. The power system oscillation phenomenon are brought up later in Section 2.5 after introducing the functionalities of the PSS.

There are several classifications of PSS, utilizing multiple input signals, complex tuning and optimization approaches to enhance stability while not affecting other adjacent generation units for the worse [22, 23]. For simplicity, a robust power system damping functionality can be obtained by feeding back the angular speed deviation $\Delta\omega$ from the SM as an input. This is depicted in Figure 2.8 by expanding the block diagram shown in Figure 2.6 with an additional stabilizing voltage V_{stab} signal fed from the excitation system.

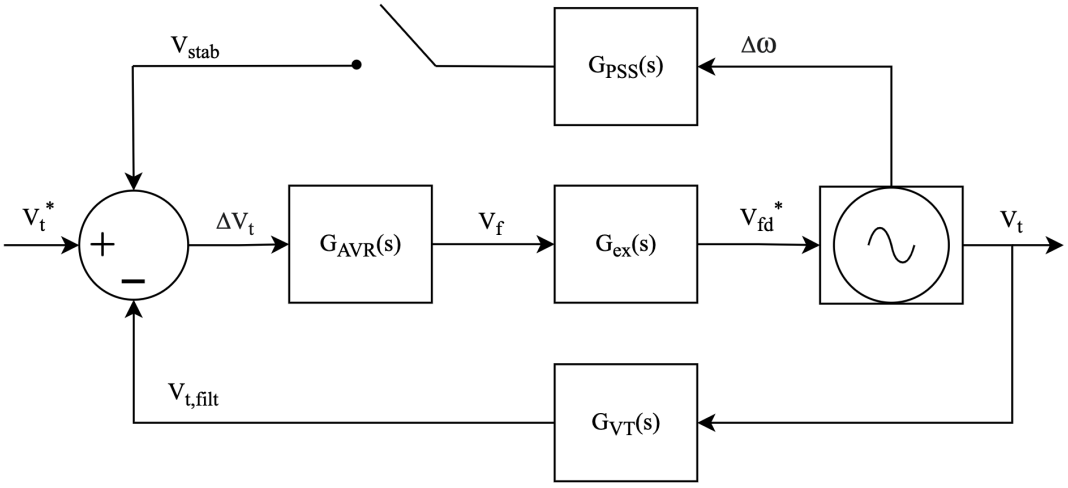

Figure 2.8: Overview of the excitation system with PSS availability.

The possibility to connect $G_{PSS}(s)$ and add additional stabilizing control when feeding back $\Delta\omega$ should provide system damping, only to the oscillation modes of interest, leaving the remaining frequency spectrum unaffected. A general block diagram is illustrated in Figure 2.9 to highlight the main features of the PSS in simplest form, and in Appendix A.1, more detailed information is provided.

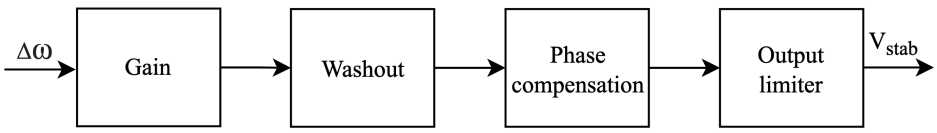

Figure 2.9: General PSS block diagram.

First in line is a PSS gain, determining the damping amplification in phase with the rotor speed deviation. Followed up by a washout block consisting of one or several high-pass filters, leaving frequency modes of higher order unchanged, without interfering with the terminal voltage in steady-state and thus also serving as a noise reducing filter.

Furthermore, the phase compensation block contributes with sufficient compensation of phase, to compensate for the slow field dynamics of the SM. Moreover, by utilizing lead-lag filters, the gain of the signal fed as input may appear in phase with the electromechanical damping torque component to mitigate the oscillations of interest [6]. Lastly, the output limiter is set as an limit to restrain too drastic fluctuations in the stabilizing voltage signal.

2.5 Power System Oscillations

The power system is continuously subjected to changes from disturbances like varying loads and change in generation that is leading to imbalances, these electromechanical mismatches result in power oscillations in the grid. Depending on the systems operating condition and ability to initiate mitigating actions, the stability could be jeopardized as a whole and the slower frequency oscillations ranging between 0.1-2 Hz are of particular interest [5].

Eigenvalues λ of an linearized system reveal how prone oscillations are to cause instability, after being determined from the **A**-matrix in state-space form around an equilibrium point. Thus, λ is obtained by computing

$$det(\lambda I - A) = 0 \tag{2.15}$$

where I is the unity matrix and the complex eigenvalues

$$\lambda = \sigma \pm j\omega \tag{2.16}$$

is characterized by a real and imaginary oscillatory part. If there exists any eigenvalues with a positive real part, the system is directly determined unstable [17]. The stability of the poles and zeroes located on the left-hand side of the spectrum can instead be observed and analyzed. The frequency of oscillations

$$f = \frac{\omega}{2\pi} = \frac{Imag(\lambda)}{2\pi} \tag{2.17}$$

are characterized by the location on the imaginary axis, while the placement of the negative real part of σ determines the system damping. The damping ratio is defined as

$$\zeta = \frac{-\sigma}{\sqrt{\sigma^2 + \omega^2}} \tag{2.18}$$

and provides an indication on how sensitive the system may be to disturbances [15].

A low positive damping ratio still implies that the system is stable, but are however more exposed to become unstable. Moreover, the undamped natural frequency mode of oscillation for a SM is defined as,

$$\omega_{natural} = \sqrt{K_S \frac{\omega_n}{2H}} \tag{2.19}$$

and describes how the synchronizing power coefficient from (2.10) influences the oscillation mode and damping ratio for changing operating conditions [6].

2.5.1 Inter-Area Oscillations

An upsetting disturbance that causes the dynamic equilibrium to cease can be followed up with continuing low frequency oscillations if the conditions allows them to. Apart from the local rotor angle oscillations, inter-area system oscillations can propagating between areas, meaning that one grid area or machine can oscillate against one another [13]. An executive summary in [24], describes the course of events causing undamped inter-area oscillation swing between grid areas in continental Europe before being damped out after mitigating action were taken. Hence, some impactful parameters influencing low frequency oscillations significantly is listed below.

Inertia time constant
In general, a SM with a greater inertia generally yield a slower system response in comparison to a smaller machine when being subjected to a small perturbation. On the contrary, the machine with larger inertia take longer time to regain steady-state due to its slower dynamics. In context of inter-area oscillations, a larger inertia constant thus tend to shift the oscillations towards the lower frequency spectrum [25].

Line impedance
Predominantly reactive impedance indirectly contributes to greater voltage phase difference between two grid areas. Each SM interprets added impedance as a longer electrical transmission distance causing weaker synchronization of the interconnection [26]. The impact of weak tie-line interconnection without power flow transmitted between two areas is observed in [27], where greater line impedance proved to worsen system damping and shift power oscillations towards the lower frequency range.

Excitation control
The supplementary addition of fast acting AVR with high gain enhance mitigating action for transient stability following a disturbance [6]. The latter two AVR properties result in a more responsive system, however with reduced electromechanical damping characteristics [7]. Higher AVR gain amplifies and broaden the frequency spectrum amplification range, including the range of low order oscillating frequencies, without proper PSS implementation [8].

3
Implementation of Study

This case study is comprised of a physical SM connected to an emulated power system with adjustable grid characteristics. The emulated grid model connected at the PCC is able to replicate varying grid scenarios by utilizing the PHIL system compatible with real-time software consisting of a simulated model [10]. The simulated model, communicating with the physical plant is developed in Simulink, using the available toolbox library `Specialized Power Systems` from Simscape Electrical. Implementation of the grid model is further explained in Section 3.2 when using a 30 kVA four-quadrant three-phase power amplifier ACS from the manufacturer Regatron [28]. A thorough overview for each step of the real-time simulation is conducted to fully comprehend how the physical grid interacts with the emulated one. This is followed by introducing the functionalities of the emulated grid and finally the tuning of the control system parameters of the emulated SM is presented after introducing the physical lab model.

3.1 Physical Lab Environment

The lab environment consists of a down-scaled three-phase 400 kV transmission system model with a power plant model represented by a SM operating in generator mode. The power plant is interconnected to the transmission system via a transformer with a voltage ratio of 400/400 V, since the entire power system is scaled down by a voltage ratio of 1:1000. There are in total six available transmission line sections and the desired amount of sections can be connected in series with the emulated PCC, this equivalent single-line diagram is illustrated in Figure 3.1.

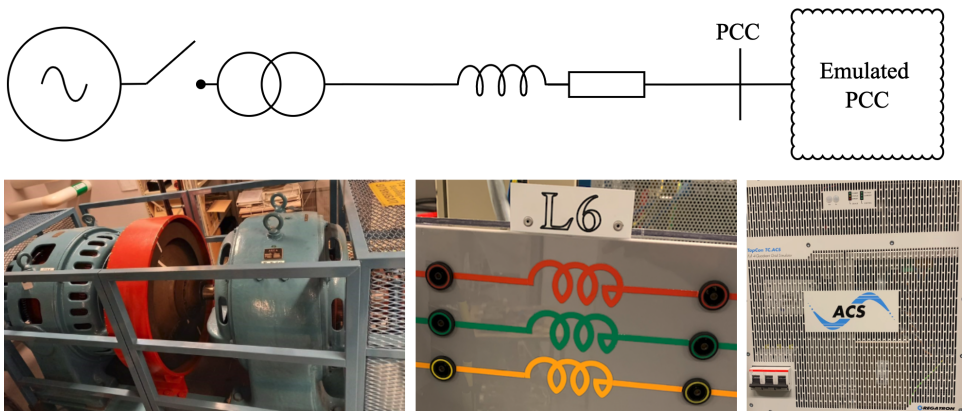

Figure 3.1: Overview of the physical lab environment.

The transmission lines are predominantly reactive with a X_{line} value of 0.953 Ω and a resistance R_{line} of 0.05 Ω. Each line represents a transmission distance of 150 km respectively. The lab environment mimics the hydro power plant Harsprånget situated along Lule river in northern Sweden, interconnected to the Nordic transmission system over long distances [29]. Moreover in the lab, the are also external loads available, consisting of industrial electric heaters with varying constant impedance loads in steps of 4.5 kW or 9 kW. Additionally shown in the single-line diagram back in Figure 3.1 is a breaker that can be operated manually from an adjacent control room. This enables safe operation and monitoring of the physical down-scaled power system.

The power plant model is a salient pole SM with three pole pairs, thus operating at 1000 rpm at rated frequency. To initiate generator mode of operation, there has to be a mechanical input and hence, a DC motor is driving the generator and is supplied through a converter operating in one-quadrant operation. Furthermore, the generator can operate in voltage regulation control through its own excitation system with the availability of power oscillation damping properties from supplementary PSS control.

To accurately represent the mechanical behavior between the prime mover and machine, there is a flywheel mounted to provide sufficient mechanical inertia [29]. The down-scaled SM in the lab has a rating of 75 kVA and the parameters are presented in Table 3.1.

Table 3.1: Parameters for physical SM used as generator.

Parameter	Value
S_n	75 [kVA]
Ω_n	1000 [rpm]
V_{LL}^{rms}	400 [V]
H	5.563 [s]
K_D	0.036 [p.u.]

Moreover, the interconnected transformer with the winding connection $Y - \Delta_{11}$ has the following parameters presented in Table 3.2.

Table 3.2: Data of physical transformer.

Parameter	Value [Ω]
R_t	0.075
X_t	0.060
R_m	$1.085 \cdot 10^6$
X_m	2866

Where R_t and X_t are the total winding impedances respectively and R_m and X_m representing the magnetization impedances.

3.2 Real-Time Interface of the Emulated PCC

By utilizing the PHIL system, the Regatron ACS is running in amplifier mode of operation and interconnects the electrical quantities in the physical lab environment with the digital counterparts inside the compiled simulated plant model [28]. Thus, interpreting the emulated and physical PCC as one, seen from the labs SM point of view. Two separate grid areas are thus formed, enabling power system oscillation phenomenons to be examined between the two areas, were the emulated grid model established inside Simulink consists of:

- One reference grid with varying grid conditions and grid strength, forming the grid characteristics.
- One power plant with changeable generation unit characteristics.

This is depicted in Figure 3.2 where the two aforementioned parts are interconnected to the emulated PCC, a more detailed description of this is provided in Section 3.3.

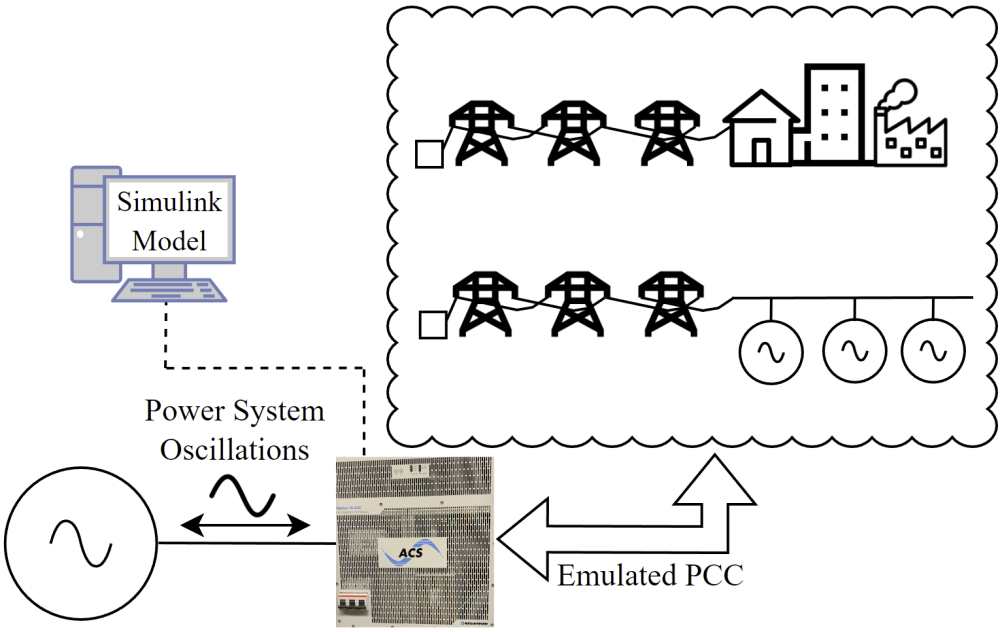

Figure 3.2: Overview of how the oscillations interact with the two grid areas.

The emulated PCC voltage is formed as a function of measured and sampled current drawn from the PCC in the lab. This is done to accurate represent the power system dynamics, with transients and disturbances instantaneously interpreted by the physical SM in real-time. Consequently, by feeding the current through a current source in the Simulink model, the emulated PCC voltage is formed with the grid characteristic of the simulated plant model.

To achieve this conversion of data, both current and voltage measurements respectively are fed as analog inputs to a MicroLabBox used for data acquisition. Through the input channels, the acquired signals are processed with the real-time interface dSPACE. This is the PHIL software compatible for model-based software integra-

tion and is processing the analog signals by converting them into digital signals [9]. Through this conversion, measured signals becomes amplified by a factor of 10, since the hardware computes every 0.1 V into a digital signal [28]. This closed loop reiterates every 200 μs for the given sampling frequency selected of 5 kHz for this study.

Moreover, to make sure that there is no path for the zero sequence current to flow for the voltage formed in case of an unbalanced scenario, the zero sequence component is eliminated. That is done for the purpose of security for both equipment and personnel. The zero sequence voltage V_0 is defined as,

$$V_0 = \frac{V_a + V_b + V_c}{3} \tag{3.1}$$

for a balanced three-phase system where each phasor has the same magnitude and phase according to Fortescue's Theorem [30]. Thus, the zero sequence voltage component can be subtracted from the emulated PCC using (3.1).

Figure 3.3 demonstrates the foregoing procedure of the real-time interface. By compiling the Simulink plant model into C-code, the converted digital signals becomes compatible with the real-time interface in dSPACE [31]. Once compiled, the model is then discretized with the given sampling frequency and thereafter operate in discrete time domain.

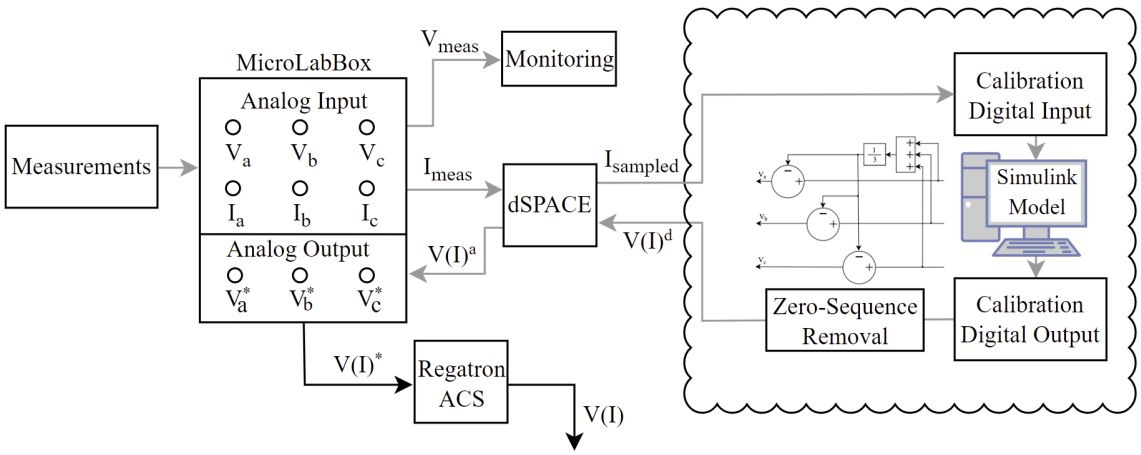

Figure 3.3: Real-time interface architecture.

Further adjustments were made on the digital signals fed as inputs to the Simulink model for calibration of the measurement equipment in such a way that the sampled data corresponds to the actual physical quantities. Similarly, before the conversion back to analog output, the factor of 10 is once again divided from the processed signal. The analog output reference is then directed to the Regatron ACS power amplifier, with rated power 30 kVA, sending out 432 V to the physical PCC for every 10 V analog voltage acquired through dSPACE [28].

3.3 Plant Model Implementation in ControlDesk

Varying grid conditions seen from the physical lab environments perspective are achieved by enabling changing parameter settings in real-time by the PHIL system. A controllable voltage source V_{ref} with the ability to alter its voltage magnitude, phase angle and impedance in real-time can instantaneously modify the PCC dynamics. Small disturbances such as frequency oscillations or voltage dips can be fabricated for changeable grid strengths Z_g. These disturbances may propagate to the physical SM in the lab over a transmission line with varying length.

The emulated grid model seen in Figure 3.2 is constructed in Simulink and after compiling it into C-code, it becomes compatible with dSPACE's experamental software ControlDesk in discrete time domain [32]. That enables graphical instrumental panels for monitoring and control, to operate the emulated grid in real-time. The complete model is shown in Figure 3.4 with the grid emulator connected. Consequently, together with the interface described back in Section 3.2, the emulated PCC is interconnected with the physical lab without any loss of information.

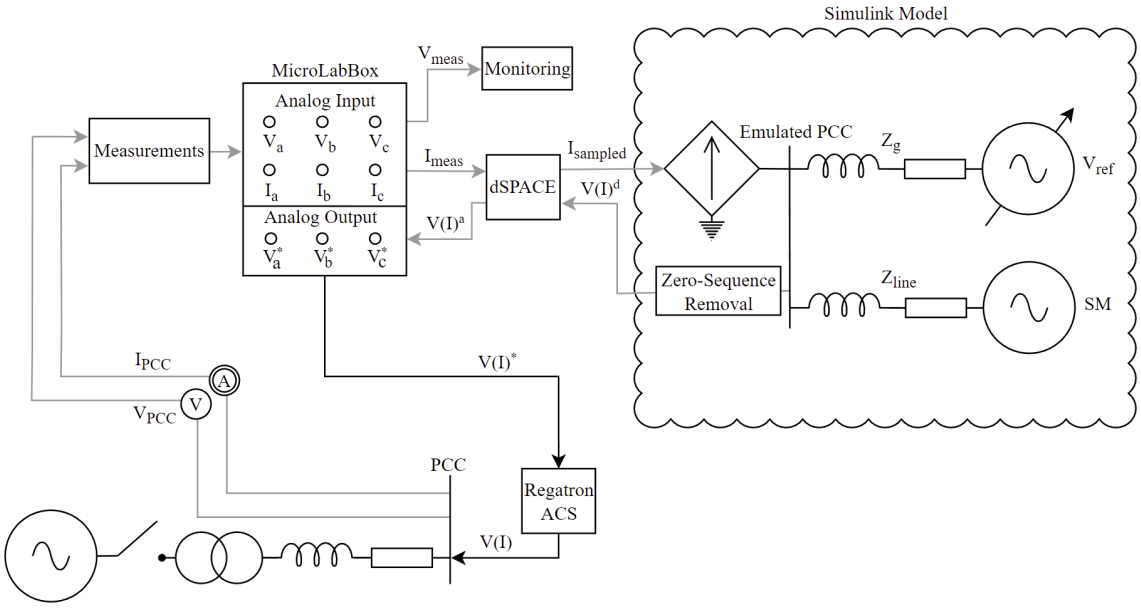

Figure 3.4: Overview of the Simulink model implemented into a real-time interface.

3.3.1 Controllable Reference Voltage Source

The formation of a balanced three-phase voltage with nominal system frequency can be done by transforming a reduced complex stationary system with two components into three-phase quantities. By applying Clarke's transformation theorem, the complex system is formed without losing any information along the way [33]. This is referred as $\alpha\beta$-frame and the voltage of the complex stationary system is defined as

$$V_{\alpha\beta} = V_{ph} \cdot e^{j\theta} \tag{3.2}$$

with the desired phase voltage V_{ph} being a vector with constant amplitude. The phase angle θ is obtained by integrating the nominal angular frequency of the system and thereafter, the balanced three-phase voltage reference is formed as

$$V_{ref} = \begin{bmatrix} V_{\mathrm{a}} \\ V_{\mathrm{b}} \\ V_{\mathrm{c}} \end{bmatrix} = \frac{1}{K} \begin{bmatrix} 1 & 0 \\ -\frac{1}{2} & \frac{\sqrt{3}}{2} \\ -\frac{1}{2} & -\frac{\sqrt{3}}{2} \end{bmatrix} \begin{bmatrix} V_{\alpha} \\ V_{\beta} \end{bmatrix} \tag{3.3}$$

through Clarke's inverse transformation. Here, K is defined as the scaling constant of the transformation and is selected as $K = 1$ for amplitude invariant scaling for this specific application, alternatively could a scaling constant be selected for RMS or power invariant scaling [19]. The plant model and controllable voltage source are thus being constructed to freely modify the following quantities:

- Voltage magnitude V_{ref}.
- Phase angle θ.
- Transmission line impedance Z_{line}.
- Grid impedance Z_g.

The first two aforementioned quantities can be modified from the complex stationary $\alpha\beta$-coordinate frame inside the controllable reference voltage source. The latter two impedances can be altered by two different approaches, which will be brought up thereafter. Consequently enabling full controllability in real-time for deterioration of the grid conditions in which power system oscillations may appear [13].

3.3.1.1 Voltage Magnitude Variation

Various contingencies in the power system such as load disturbances or temporary transient may lead to sudden drops or rises of voltage throughout the grid. Voltage variations may impact the operation of controllers such as excitation systems of generation units interconnected to the same PCC and the significance of voltage variations increases further for weaker grid connections [34].

To access and alter the reference voltage magnitude V_{ref} in Simulink in real-time through ControlDesk, a specific control method is developed. This since the parameters inside the blocks used from Simulinks library are inaccessible once the model is compiled into C-code and is up and running. The use of *gain-blocks* with a unique identification name can instead be accessed from ControlDesk in real-time.

The general procedure on how this is done is illustrated in Figure 3.5 with the *gain-block* being accessible live. From the gain, the signal can be altered through a numerical input in ControlDesk while the output can be monitored. This gives the operator some degree of freedom to vary the designed grid conditions during testing without needing to shut down and recompile.

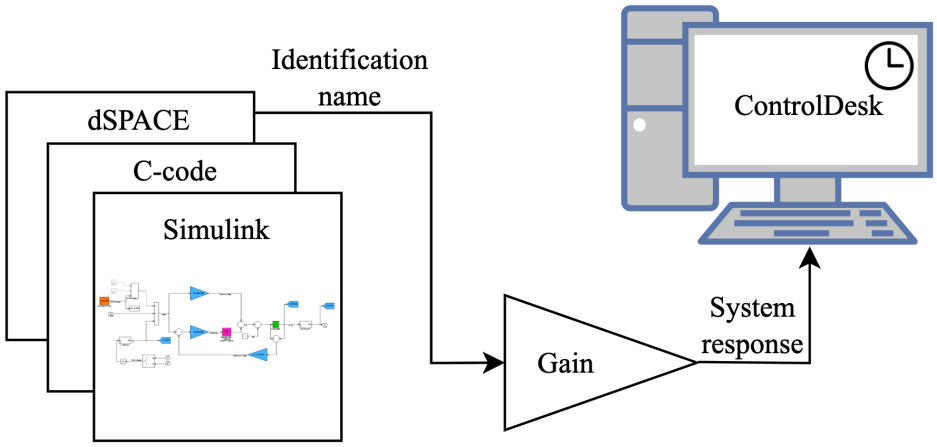

Figure 3.5: Overview of accessing parameters in ControlDesk real-time.

To initiate a change in voltage magnitude whilst making it restore itself back to nominal voltage for a prespecified time period, the design presented in Figure 3.6 is used where the changeable blocks are highlighted in color. Initially the *gain-block* with identification *V_drop_signal* is set to 0 and nominal voltage is maintained. Once the signal is initiated by inputting a 1, the following events take place:

1. The threshold of the switch is set to operate once the lower branch is greater than 0.1. The logic senses that the signal is in fact 1 and the switch switches to false. Thus, passing through a gain equal to the desired voltage variation in p.u. identified in *V_ref_drop*.

2. The signal threshold signal is fed through a *on delay-block* named *V_drop_time* with a predefined time delay. This time delay resets the signal back to its initial condition value and restores nominal voltage in an instant.

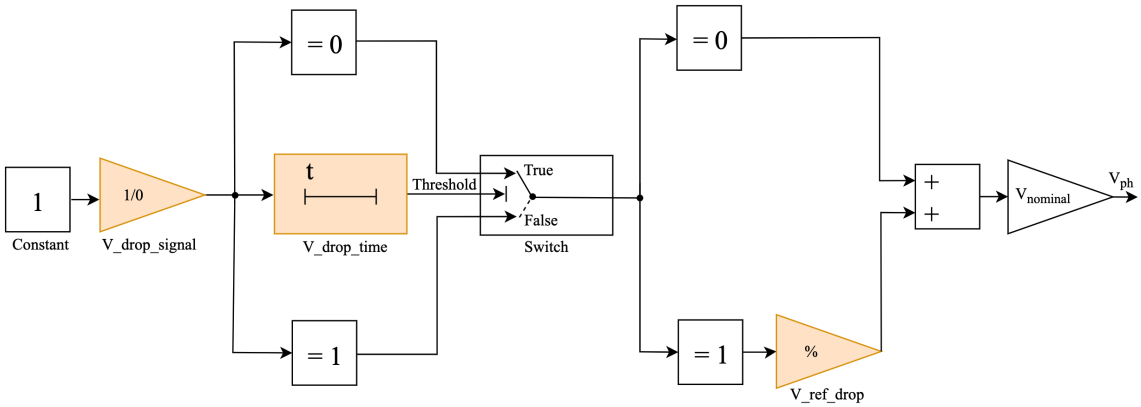

Figure 3.6: Block diagram of voltage magnitude variation.

3.3.1.2 Phase Angle Jump

Arbitrary small shifts in phase angle θ can cause sufficient active power imbalances in the three-phase power system. This type of instability can be designed in the $\alpha\beta$-frame when adding a detrimental step response added to the phase angle. Figure 3.7

presents a schematic overview of (3.2) with the addition of a phase angle jump accessible from ControlDesk, where the gain *Phase_jump_signal* is initially set to 0, meaning that the controllable reference voltage source is operating at nominal frequency. Once the signal is set to the desired phase jump (e.g., -10° or -20°), the following events occur:

1. The constant of 1 to the far left in Figure 3.7 is multiplied with the desired phase jump, sensed and sampled through a low-pass filter with a time constant inversely proportional to the nominal electrical frequency ω. This is for the purpose of obtaining a first order response.

2. This shift in phase angle is converted into radians and added to the rotating nominal phase angle, causing a direct shift, in turn initiating a change in rotor angle for the interconnected machines.

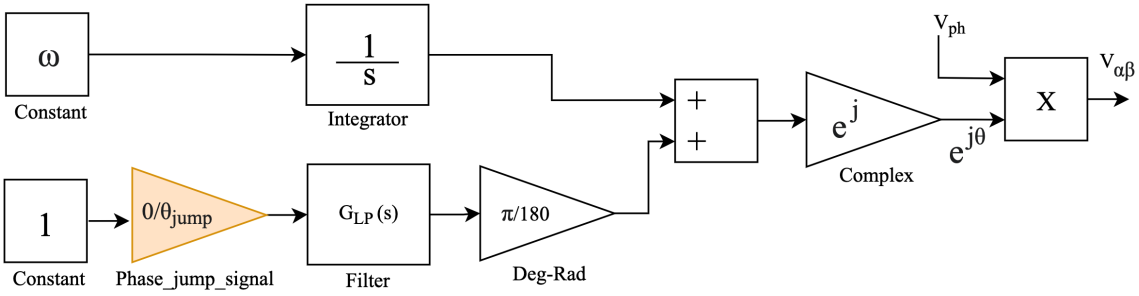

Figure 3.7: Block diagram of phase angle jump.

3.3.2 Changeable Transmission Line Distance

The physical transmission line sections available in the physical lab environment are needed to be assembled prior to grid energization, more flexibility is added by implementing emulated replicas. This enables a more user friendly experience while enhancing personal safety. A total of six transmission lines is accessible in the lab, once emulated, the lines are instead connected inside the emulated grid. The design approach applicable with the user interface in ControlDesk is shown in Figure 3.8.

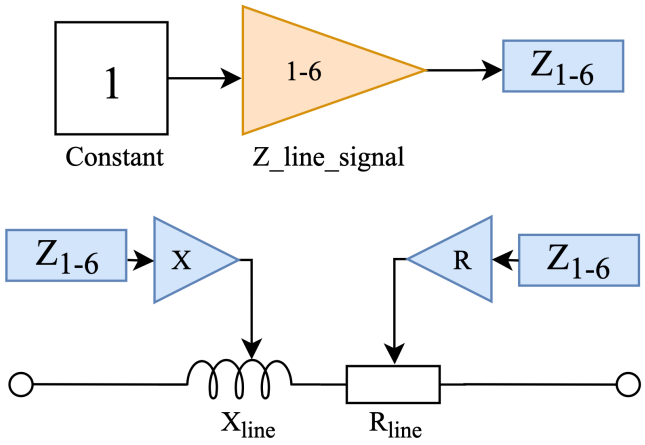

Figure 3.8: Block diagram of changeable line impedance.

The desired number of transmission lines connected in series is specified inside the *Z_line_signal* gain. An input signal between (1-6) is routed through Z_{1-6} and simultaneously multiplied to both elements and thus, enabling access to vary the emulated line impedance in real-time.

3.3.3 Variable Grid Strength

By modelling the controllable reference voltage source behind a grid impedance, the emulated PCC is seen as weaker from the rest of the grids perspective. One implication with the existing configuration seen in Figure 3.4 once implemented in Simulink is emerging with the grid impedance Z_g, since it is connected in series with the modelled current source. The inductance is a current stiff element, thus also considered as a current source by the software from its characteristic equation [35]. The coexistence of two in series makes it so that the simulation gets stuck in an infinite algebraic loop.

An alternative solution to circumvent this, is by implementing a high value resistance in parallel between the two without losing accuracy of the model representation. However, a large parallel resistance leads to longer computational time for each sampling period, whereas a too low resistance value results in a high simulated power consumption. A trade-off between the two options are to select a arbitrary resistance in parallel and compensate the voltage drop so the emulated PCC maintain its nominal voltage in an unloaded condition. By representing the variable voltage source as an Thevenin equivalent circuit together with the parallel resistance R_p, the desired grid impedance can be obtained from the circuit illustrated in Figure 3.9.

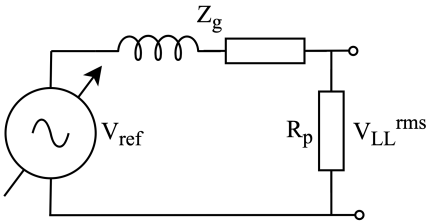

Figure 3.9: Thevenin equivalent circuit.

Thus, the equivalent grid impedance is defined as

$$Z_g = \frac{R_p Z_{th}}{R_p - Z_{th}} \tag{3.4}$$

for given Thevenin impedance Z_{th} inserted by the user in ControlDesk. This defines the grid strength of the emulated PCC. In order to make sure the voltage is kept to its nominal value V_{LL}^{rms} of 400 V, the reference voltage is set to

$$V_{ref} = V_{LL}^{rms} + Z_g \frac{V_{LL}^{rms}}{R_p} \tag{3.5}$$

with phase shift $\angle V_{ref}$ of the voltage angle taken into consideration, to compensate the voltage drop. Consequently, when there is no current flowing in the circuit, nominal voltage at the emulated PCC remain unchanged.

3.3.3.1 Verifying Variable Grid Strength in Simulation

Verification of the complete plant model to operate as intended prior to energization in the physical lab environment is done with a replica constructed in Simulink. By running the simulation model in continuous time domain with a system base of 30 kVA, the grid strength of the emulated PCC is examined by applying varying system loading.

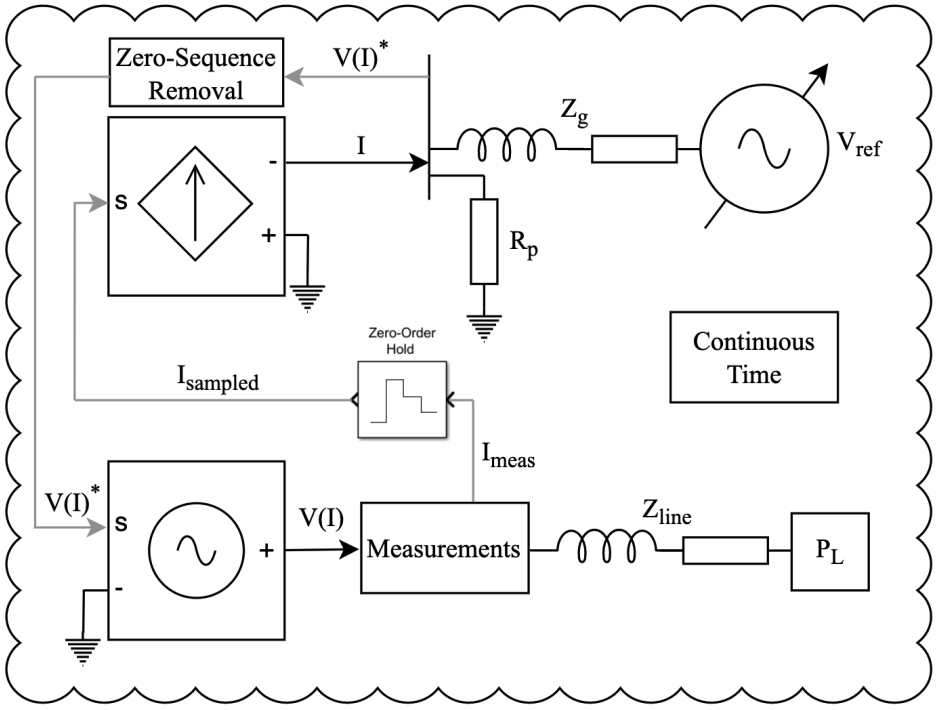

Figure 3.10: Simulink model implemented in continuous time domain simulation.

The overview of this is shown in Figure 3.10 and the procedure is the following:

1. The lab configuration consists of one transmission line section equal to the one in the lab environment, as well as one resistive load P_L. At first the system is running unloaded and after 0.2 s the system is loaded with 4.5 kW, then after 0.4 s the total load is 9 kW.
2. Current measurements acquired from the grid are sampled at predetermined sampling frequency 5 kHz using the block `Zero-Order Hold` found in the Simulink library. Sampled current is fed to the emulated grid model through a reverse connected current source to draw current from the emulated PCC.
3. The emulated grid model consists of a grid impedance and equivalent controllable voltage source with adjusted magnitude and compensated phase angle shift. It is forming the reference voltage $V(I)^*$ as a function of external load current drained through the emulated grid impedance.
4. The formed output voltage from aforementioned step is fed via the block subtracting the zero-sequence component and fed back to the grid through a voltage source. Each step is then reiterated for every sampling period and measurements are observed.

The outcome of this is shown in Figure 3.11 where voltage and current from the measurement-block are presented in p.u., with respect to a system base of 30 kVA. The voltage and current plots were obtained by selecting the following parameters:

- $R_p = 16\ \Omega$.
- $Z_{th} = 0.4 + j2\ \Omega$.

The parasitic resistance in parallel is consuming 10 kW active power at nominal voltage. From (3.4), the grid impedance is calculated as $Z_g = 0.15 + j2.07\ \Omega$ from the Thevenin equivalent circuit in Figure 3.9. Furthermore, the compensated reference voltage is calculated to $V_{ref} = 407\angle 7.3°\ V$ from (3.5) and thus, the correct voltage is obtained at the emulated PCC once the system is unloaded. The grid impedance causes the reference voltage to drop as a function of system load demand and this impedance can instantaneously be altered or switched on and off in real-time.

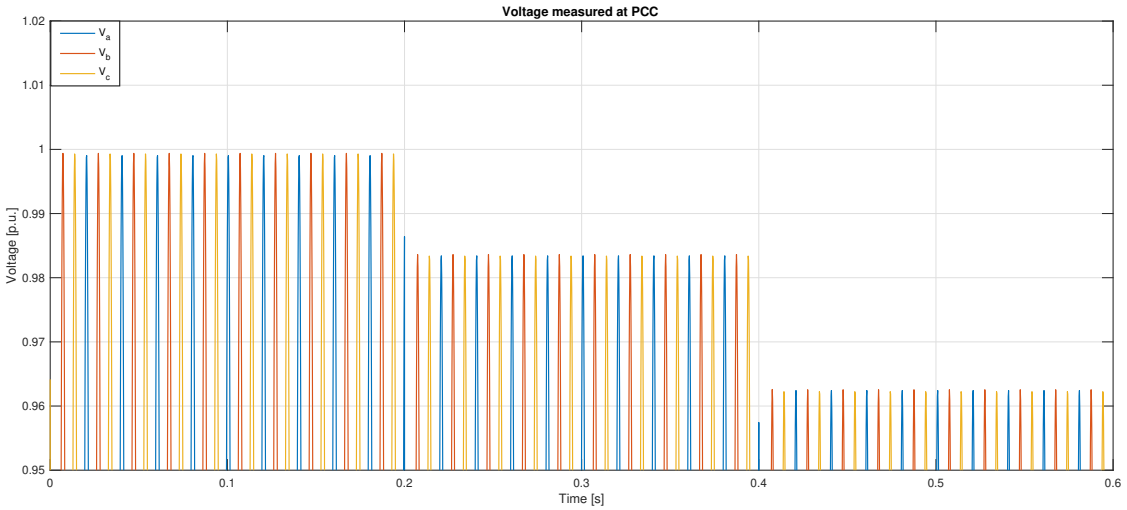

(a) Measured voltage [p.u.].

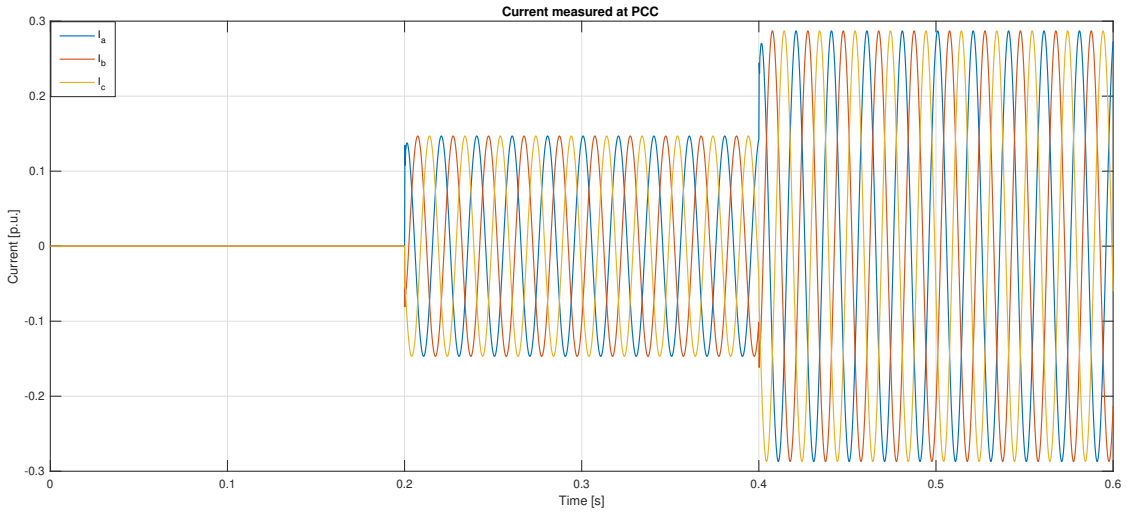

(b) Measured current [p.u.].

Figure 3.11: Measurements at PCC.

3.4 Emulated Synchronous Machine

Power oscillation dynamics can emerge from the emulated PCC with the addition of a SM in the Simulink model, as seen in Figure 3.4. One of the methods of modelling the SM is to use the `Synchronous Machine pu Standard` model from Simspace Electricals library, built on a sixth-order electrical state-space model [36]. For consistency in relation to the physical machine, the dynamics of the emulated SM are also represented as a salient-pole machine. The parameters of interest affecting oscillatory tendency of the emulated SM connected to the PCC include:

- Rated power S_n and inertia constant H.
- Series impedance interconnecting the emulated SM to the PCC.
- Machine loading condition in relation to rated power.
- AVR gain of excitation system.

Moreover, the dimensions of the emulated SM added should be oversized in relation to the physical SM in the lab with a rating of 75 kVA, to initiate slower oscillating system dynamics [16]. Hence, the inertia constant of the emulated machine is automatically re-scaled according to its definition from (2.3) when scaling to a new system base.

3.4.1 Machine Reactance Characteristics

As mentioned in Section 2.1, the field windings magnetic flux is aligned along the d-axis reference frame, where the magnetic reluctance is the lowest from the salient-pole geometry. Hence, the d-axis synchronous reactance X_d is greater than the q-axis counterpart X_q.

During transients or faults however, the equivalant reactance is different because there is current induced in rotors field and damper windings to maintain the flux linkage. Figure 3.12 below is showing each equivalent circuit during their state, X_D being the flux path around the damper windings, X_f the path around the field winding. In steady-state, it is only along the armature reactance X_a flux path and leakage reactance X_l [37].

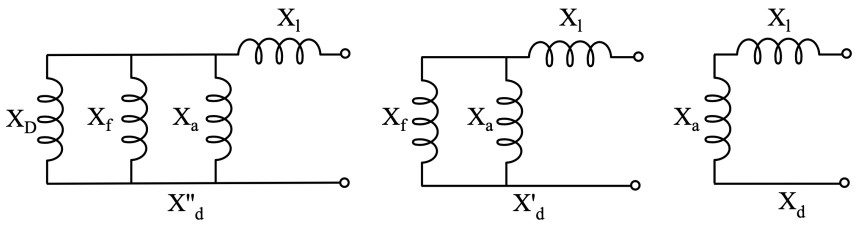

Figure 3.12: Illustration of the equivalent SM reactances shown in subtransient, transient and steady-state (left to right).

Consequently, the circuits are transitioning from a subtransient state, back to a steady-state reactance, Table 3.3 presents the parameter values used for the emulated SM model.

Table 3.3: Parameters for the emulated salient-pole SM.

Parameter	Value [p.u.]
R_s	0.003
X_l	0.15
X_d	1.1
X'_d	0.25
X''_d	0.2
X_q	0.7
X''_q	0.2

According to [6], the subtransient time period lasts for 1-3 cycles, whereas the transient state typically lasts up to 10 electrical cycles. The typical relation between the d and q-axis for salient-pole SMs given in [14] states that $X_d > X_q$ and $X''_d \approx X''_q$ as a rule of thumb.

3.4.2 Parameter Tuning of the Emulated SM

The PI-controller parameters of the AVR are set in order to provide the field excitation needed to regulate the terminal voltage of the machine. When operating in steady-state, a small disturbance signal initiating a deviation from the reference set-point is sufficient to cause imbalance in the regulator. The emulated SM is first decoupled from any grid forming connection point to freely set the grid conditions from the machine itself. From there, the system response of the AVR can be set to have a desired behavior [15]. This can be achieved by connecting the electrical output of the machine in generator mode of operation to a resistive load.

However, letting the SM regulate the system frequency requires a turbine governor to control the rotor speed coupled with the system frequency. A turbine governor is thus feeding back the rotor speed and compares it to a desired reference set-point, Figure 3.13 shows the combined block diagram.

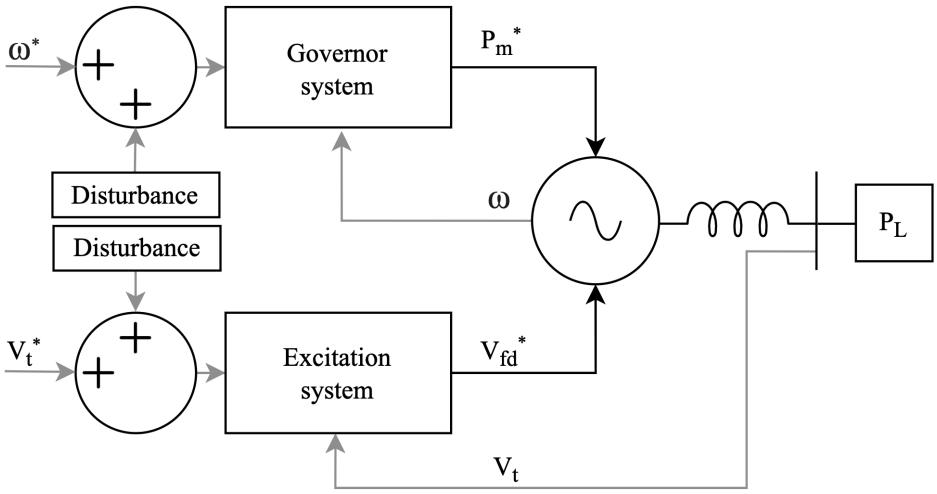

Figure 3.13: Test system for tuning controllers given a reference disturbance.

Much like the excitation system, the governor is also a system containing a regulator to restore system frequency. In simplest terms this may also be done using a PI-controller, as seen in Figure 3.14.

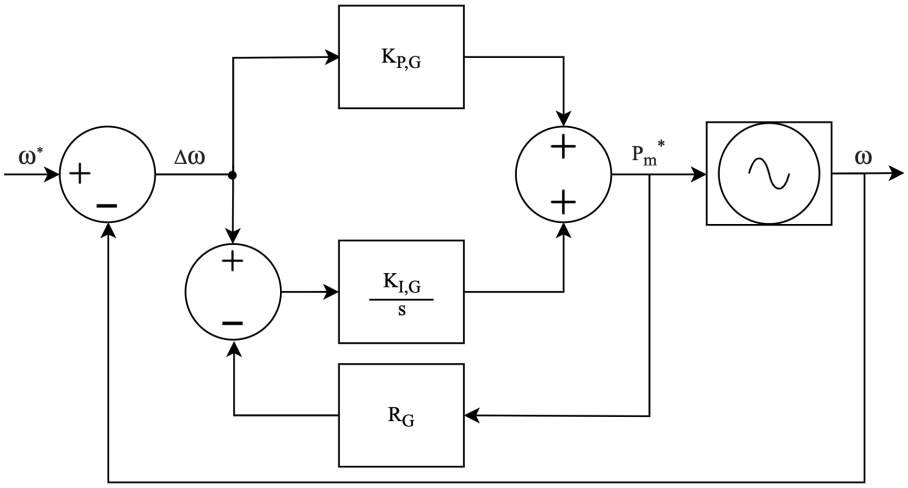

Figure 3.14: Governor system block diagram.

The speed-droop characteristics are obtained by adding a governor droop constant R_G, accounting for a small gain of power for every change in frequency. This is usually given in percent, ranging from 3-5 % and is considered as a regulation constant [14]. Thereafter, the PI-controller of the AVR is tuned once the governor yields a reasonable slow system response to regulate and restore equilibrium.

3.4.2.1 Tuning of the Turbine Governor System

The aforementioned governor turbine system is first initiated alone without any inherent excitation dynamics for the emulated SM. Consequently, the machine field voltage remains constant from the converged machine-initialization solution in steady-state. This is for the purpose of first tuning the parameters of the governor without any influence from the faster AVR, the parameters of the turbine governor is presented below in Table 3.4.

Table 3.4: Parameters for the governor system.

Parameter	Value [p.u.]
ω^*	1
R_G	0.03
$K_{P,G}$	5
$K_{I,G}$	1

As shown in Figure 3.13, the governor reference input is subjected to a small step disturbance. Moreover, the interconnected resistive load is rated half the capacity in relation to the machine, hence the output power of the emulated machine is 0.5 p.u. in steady-state.

The following sequence of events take place in Figure 3.15:

- t = 40 s: A step disturbance of -0.02 p.u. is initiated at the frequency reference.
- t = 80 s: The disturbance is cleared by adding 0.02 p.u. to regain steady-state.

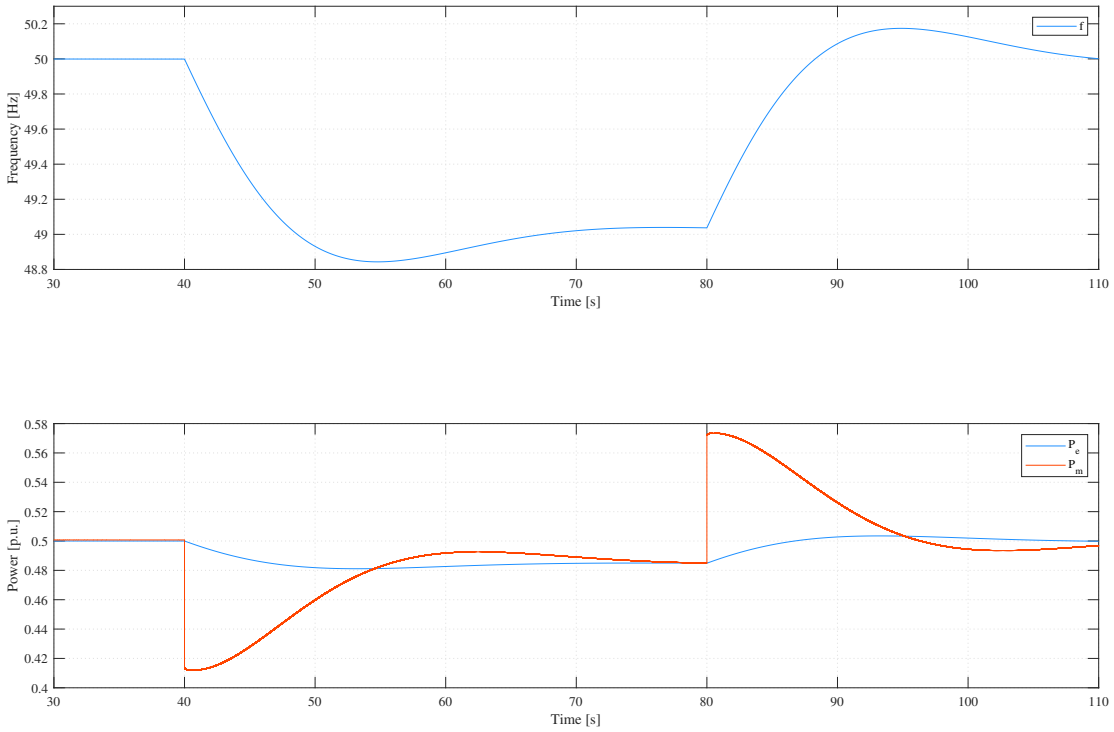

Figure 3.15: Governor system response when being subjected to small disturbances.

Being observed is a decrease in the frequency set-point, causing the mechanical power of the SM to decrease and then successively increase back towards the new operating point. The turbine governor regulator dynamics demonstrated are slow enough to observe some overshoot before settling. Additionally, the slow response in mechanical power is reflected in the frequency.

3.4.2.2 Tuning of the Excitation System

Following the tuning of the turbine governor, the frequency eventually regain steady-state following a system upset. Instead of initiating a disturbance at the governor reference, a small deviation is set at the terminal voltage reference to observe how the field voltage is regulated by the AVR, Table 3.5 lists the parameter values for the regulator and exciter limiter.

Table 3.5: Parameters for the excitation system.

Parameter	Value [p.u.]
V_t^*	1
$K_{P,AVR}$	15
$K_{I,AVR}$	15
$K_{aw,AVR}$	10
V_{fd}^{max}	2.5
V_{fd}^{min}	-2.5

The exciter, consisting of a first order low-pass filter has a time constant T_{ex} of 10 ms to obtain a fast system response. By instead running the system in no-load, the resistive load will marginally impact the system frequency by the change in terminal voltage. Figure 3.16 shows the resulting system behavior with the addition of the excitation system and similarly, the following events take place:

- t = 30.5 s: A step disturbance of -0.02 p.u. is initiated at the terminal voltage reference.
- t = 35.5 s: The disturbance is cleared by adding 0.02 p.u. to regain steady-state.

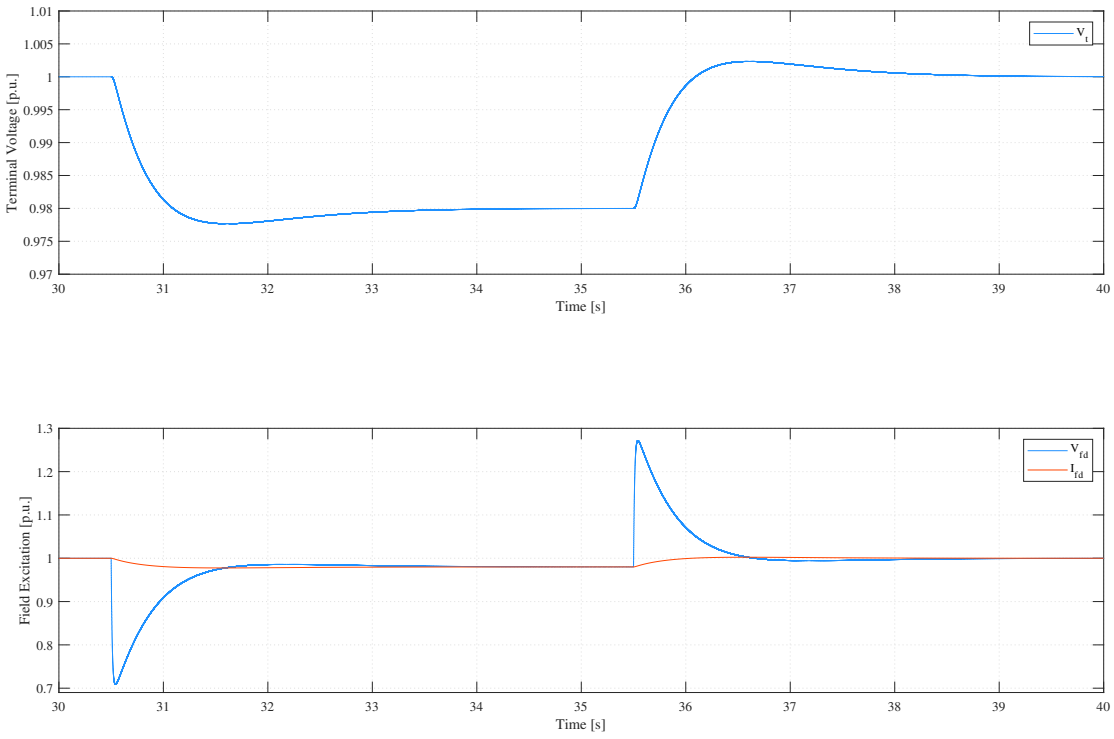

Figure 3.16: Excitation system response when being subjected to small disturbances.

Once the terminal voltage reference is altered by 2 % the field current follow suit, followed up by some slight under/over-shoot from the regulated field voltage. The modelled behavior of the static exciter mimics a first order system response.

4

Simulation of Power System Oscillations

This chapter introduce inter-area interactions between the two grid areas, after setting the grid conditions in each area independently to fabricate a distinct resonance peak within desired frequency range. Through phasor domain simulations in Simulink, the complete system setup is built-up and linearized to examine the systems frequency response.

4.1 Overview of Inter-Area Oscillations in Simulink

Before performing the actual lab tests, the expected conditions for power oscillations are produced in an simulation environment. To present and analyze the system damping in bode diagrams, the model is linearized around a stable operating point. The physical model together with the emulated grid presented back in Chapter 3 is built up in Simulink with the intention of setting the right grid conditions for inter-area oscillations and Figure 4.1 illustrates this setup. Examining small perturbations around a stable system equilibrium point is done using a linearization tool from Simulinks external software package `Simulink Control Design` [38]. The systems state of stability can thus be examined by analyzing the frequency responses once linearized.

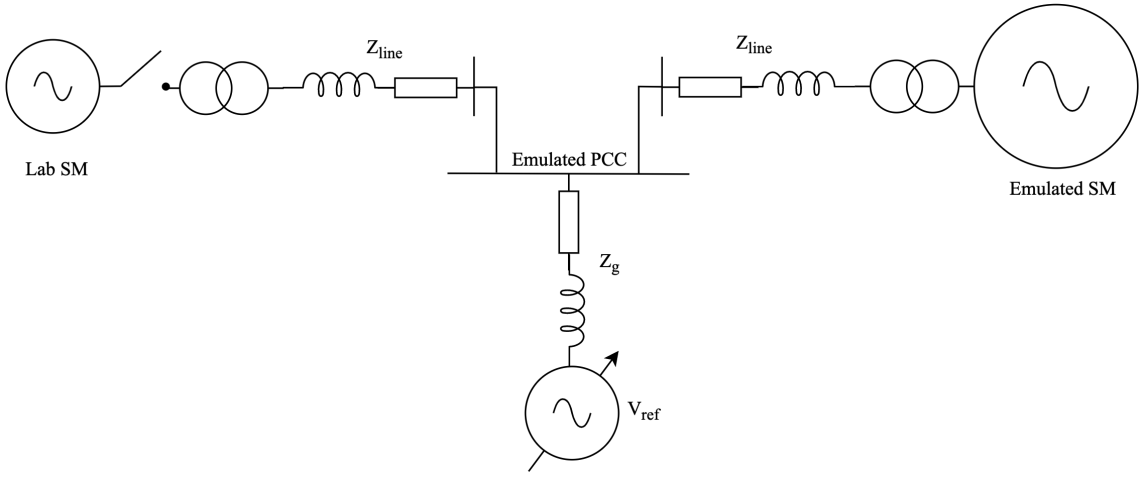

Figure 4.1: Simulation setup of the emulated and physical network.

The main approach on initializing inter-area oscillations is to first fabricate power swings between a relatively large emulated machine and a fixed grid connection that is characterized by a specified grid strength. This grid acts as a reference swing-bus, representing an adjacent grid area that is absorbing the power sent to it [15]. The influencing grid parameters, setting the right conditions for power oscillations to arise are first investigated. Thus, providing information about what modes of oscillation to expect in the physical lab setup and the mode of oscillation can thereby be tuned to the desired resonance peak in advance.

Henceforth, similar repetitive approach is done with a simulated representation of the physical lab model. Again, the parameters affecting the grid conditions causing low frequency oscillations are altered, instead of only focusing on the slightly faster local modes of oscillating phenomenons. Consequently, the objective is to form a good understanding on the stability boundaries of the machine in the lab when oscillating towards the emulated grid.

Lastly, the two aforementioned setups are interconnected and the influence of inter-area oscillations between the lab environment and emulated grid are investigated. Thereafter, the mitigating action provided by a supplementary PSS is observed, the model and parameters implemented is presented in Appendix A.1. To sum up, the simulation methodology are the following:

1. Initiate inter-area power oscillations between the emulated SM and emulated PCC.
2. Investigate local swings of the physical SM when being connected to the emulated PCC.
3. Interconnect the two machines in both grid areas to investigate swings against each other according to Figure 4.1.

4.2 Frequency Response of Power Oscillations

The system amplification response of power system oscillations over the frequency spectrum of a machine is obtained by analyzing the voltage input, to electrical power output. When the AVR is implemented, the reference voltage V_t^* is initiated as system input and without the AVR, the calculated constant field excitation voltage is instead utilized as system input [5].

By using Simulinks machine initialization tool after running the power flow, the correct initial conditions are calculated and set for the SM [35]. This can be compiled and run in Simulink in either continuous, phasor or discrete time domain. Thus, enabling Simulinks linearization tool to linearize the system around a predetermined operating point. The frequency response is then obtained by the linearization software when it injects a sinusoidal signal of constant amplitude with varying frequency over a specified spectrum into the linearized system [16]. This response is presented in a logarithmic scaled bode diagram, consisting of magnitude and phase over the formed transfer functions swept frequency range.

4.2.1 Emulated Synchronous Machine with Constant Field Magnetization

The emulated SM is connected to the emulated PCC via a fictional transformer and variable line impedance, as depicted in Figure 4.2. The emulated SM is rated three times greater than the nominal power of the SM in the lab, i.e., 225 kVA and consequently, the inertia constant H is re-scaled to 1.1854 s, using (2.3).

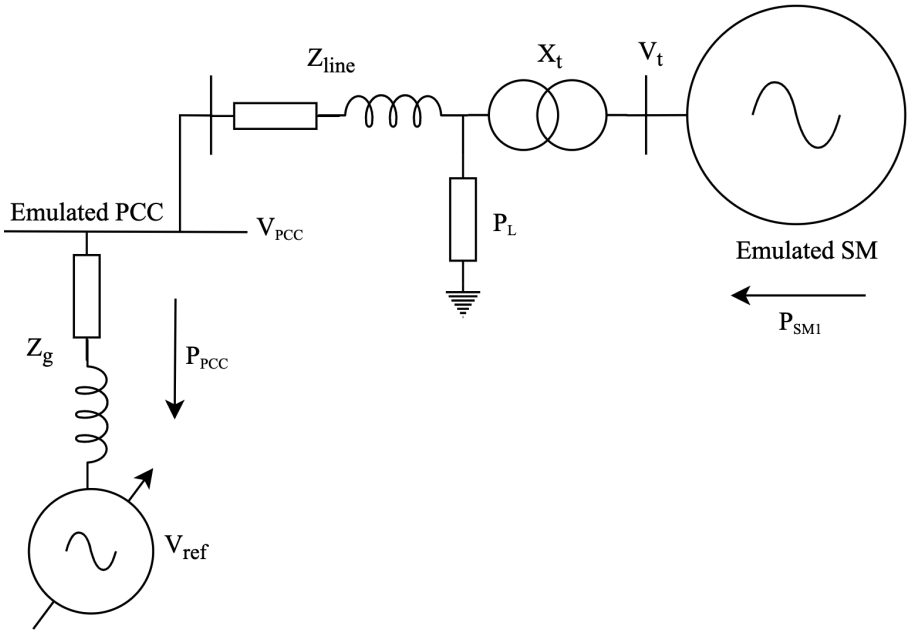

Figure 4.2: Simulation of the emulated SM connected to the emulated PCC.

Parameters of the emulated grid are specified in Table 4.1 with respect to the system base of 225 kVA. The reactance of the fictional transformer is set to the specified constant value, since the component is inaccessible in real-time simulation. The loading condition P_L of the emulated SM is set equal to half capacity and for consistency throughout the Simulink simulation tests prior to the physical lab results, no active power is being transmitted to observe each parameter without interference.

Table 4.1: Simulation parameter data for 225 kVA rating.

Parameter	Value [p.u.]
P_{SM1}	0.50
P_L	0.50
X_t	j0.10
Z_g	0.03 +j1.00

The upcoming frequency response test results evaluates the following parameters, one at a time for the emulated machine:

- Inertia time constant.
- Line impedance.

4.2.1.1 Influence of Inertia Time Constant

The influence of machine inertia is evaluated without any line impedance when connected to the PCC with grid impedance Z_g. The impact of system inertia is shown in Figure 4.3, when being incrementally multiplied by the given factor. The phenomenon of interest when analyzing the bode diagrams is the peak in magnitude, followed by a step down in phase [16]. This will further on be referred to as the frequency resonance peak. As seen here originally, the three times larger machine with nominal inertia constant has a resonance frequency around 1 Hz.

The inter-area oscillations initiated by this machine should ideally be of slower characteristics in the lower frequency range. That is to initiate a second resonance peak observable from the physical machines point of view. Hence, a larger inertia constant factor are of interest. Moreover, the magnitude increases with greater system inertia [5]. Meaning that the oscillatory inter-area swings are expected to contribute more to dynamic interference of slower power oscillations once interconnected with the physical machine in the lab.

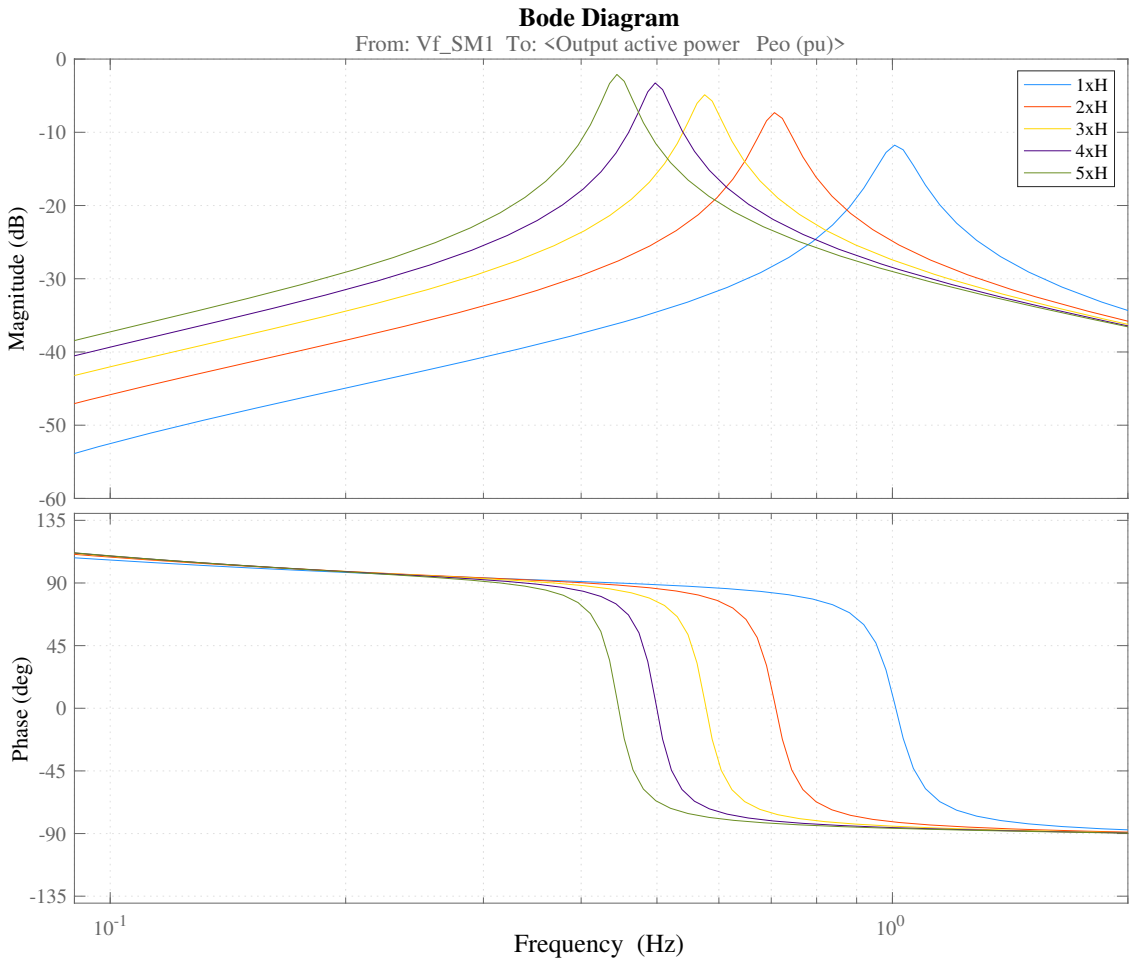

Figure 4.3: Bode plot from constant field voltage to output power of emulated SM with varying inertia constants.

4.2.1.2 Influence of Line Impedance

Similar evaluations are observed by varying the line impedance. The system impact is shown in Figure 4.4 and corresponds to one to five emulated transmission line sections being connected in between the emulated machine and PCC. For illustrative purposes in this frequency response shown, the inertia constant has been multiplied by a factor of three after evaluating the inertia constants impact. When only interconnecting one transmission line section, the power oscillations dynamics are shifted drastically to the left when comparing with 3xH in Figure 4.3. Even more so, connecting more transmission line sections weakens the interconnection and shifts the resonant frequency response towards the lower frequency range. Resulting in a slightly more responsive system with lower damping. This phenomenon was expected according to [27], even without any transmitted power flow. Hence, weaker tie-lines severely influenced the impact of inter-area oscillations. For a given inertia constant of the over-sized emulated machine, the desired mode of inter-area oscillations can be obtained by varying the line impedance. One emulated transmission line section is sufficient to obtain a resonance peak without jeopardizing system stability.

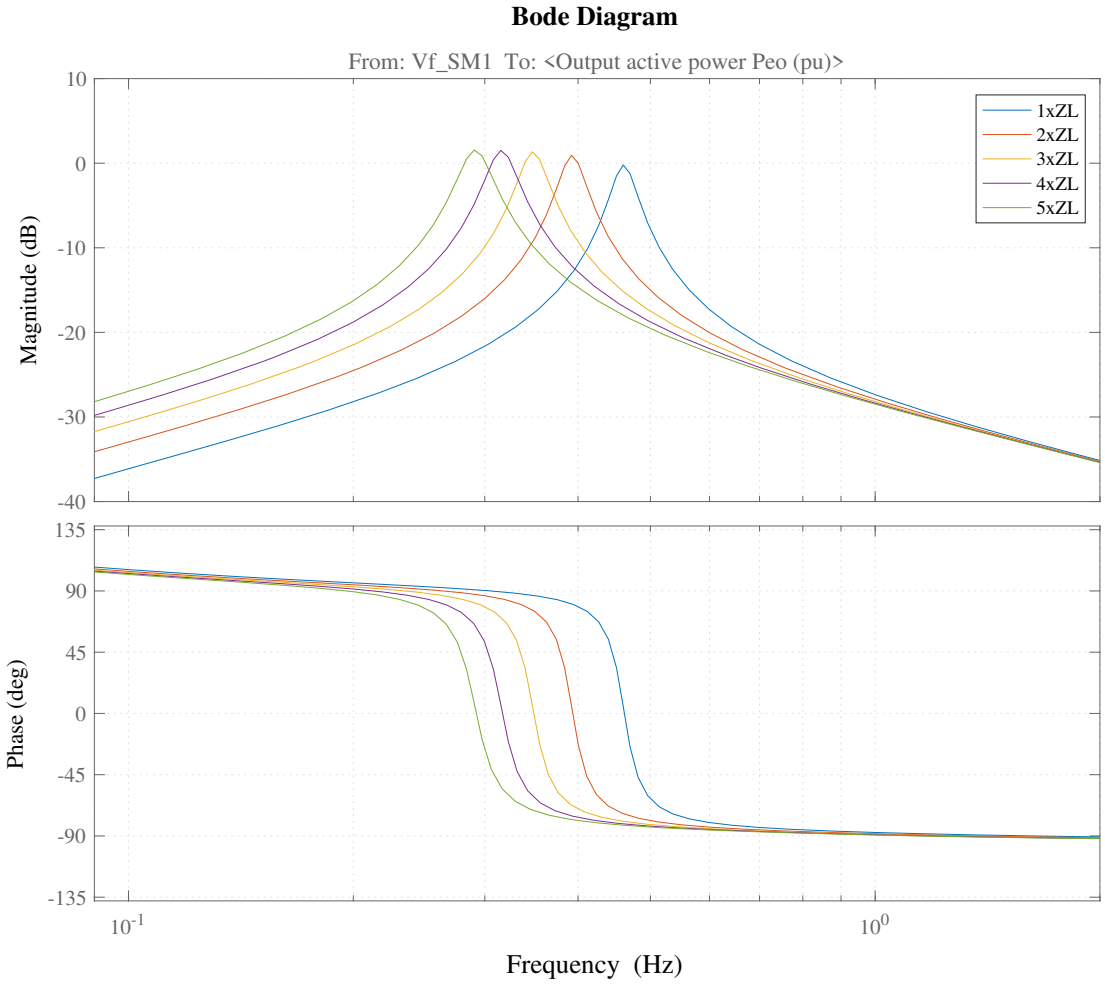

Figure 4.4: Bode plot from constant field voltage to output power of emulated SM with varying line impedance interconnection.

4.2.2 Physical Synchronous Machine Local Mode of Oscillation

Local power swings are investigated for the physical machine in the lab through simulations. Figure 4.5 illustrates the corresponding scheme when connected alone to the emulated PCC, while the parameters of the physical transformer, rated 75 kVA are presented in Table 3.2 in Section 3.1.

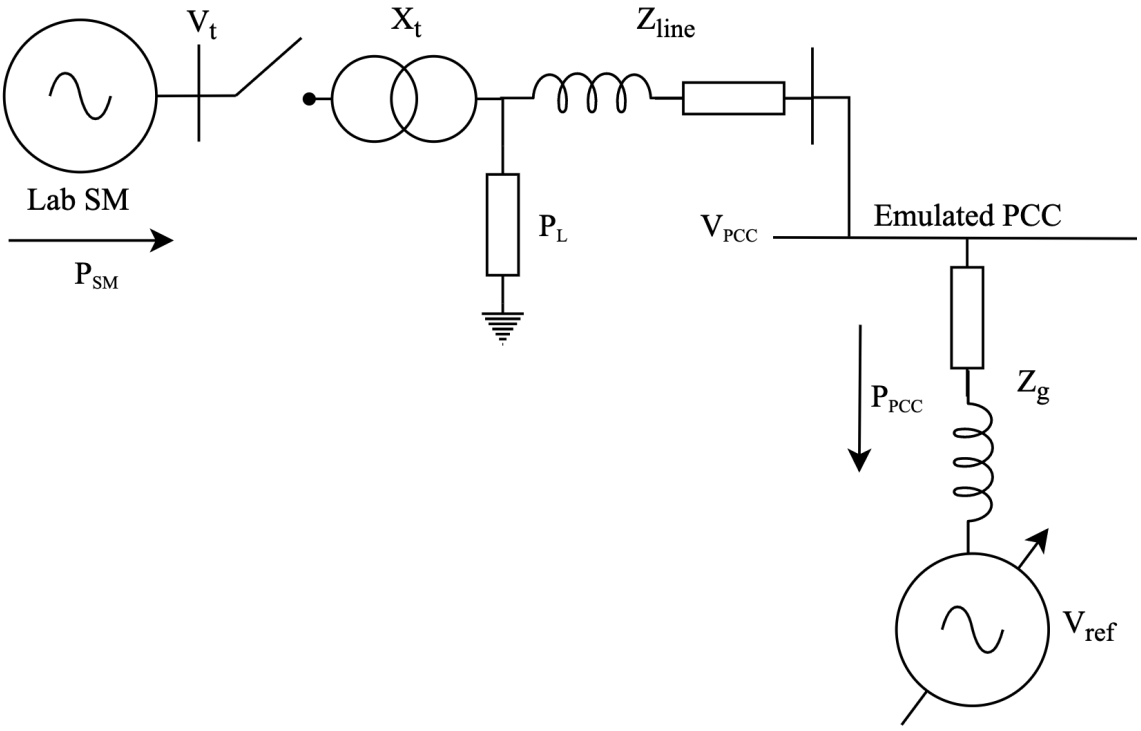

Figure 4.5: Simulation of the SM in the lab connected to the emulated PCC.

Similarly as the emulated machine, the local loading P_L of the machine and output power P_{SM} are assumed to be constant 0.5 p.u. with respect to rated system base. This is not the conditions for the physical tests performed later on, but for illustrative purpose in the simulations, it is kept constant. In fact, the local swings are greatly influenced by the loading, as well as power flow transmitted [6], [27]. However, the simulated frequency response results presented are more of an approximation on what to expect in the physical lab.

Moreover, increasing the line impedance caused the resonance peak to appear further to the left, i.e. in the lower frequency spectrum. This was observed back in Figure 4.4 and is not desired to highlight local swings. The line impedance is therefore set as low as possible to obtain a faster responding system response in the vicinity closer to 1 Hz without causing instability. Consequently, the emulated line impedance between the physical SM and emulated PCC is set to half a transmission line. This is equivalent to 75 km in electrical transmission distance, representing a shorter interconnection when comparing with the emulated SM. Furthermore, the reference grid still has the same grid impedance, as specified in Table 4.1.

The physical machine have the possibility to mitigate power oscillation swings by adding a PSS to the excitation system. Hence, the impact on the power response in frequency domain is conducted with the addition of an AVR. Figure 4.6 compares the frequency response of the physical machine with and without the AVR. The more responsive outcome is depicted with the red curve, where a higher system gain and fast excitation result in a different transfer function for the system, with the parameters of the AVR presented back in Table 3.5.

The peak in magnitude is still accompanied by a step down in phase, considering it to remain stable [8]. Since it now is more responsive, it may however also be more sensitive to power oscillations. The resonance peak occur around 0.7 Hz for both responses, which is considered quite low for local swings [5]. However, considering the current loading of the machine, without any active power transmitted, the peak is expected to be situated a bit further to the right in the frequency spectrum in the physical lab environment, according to (2.19).

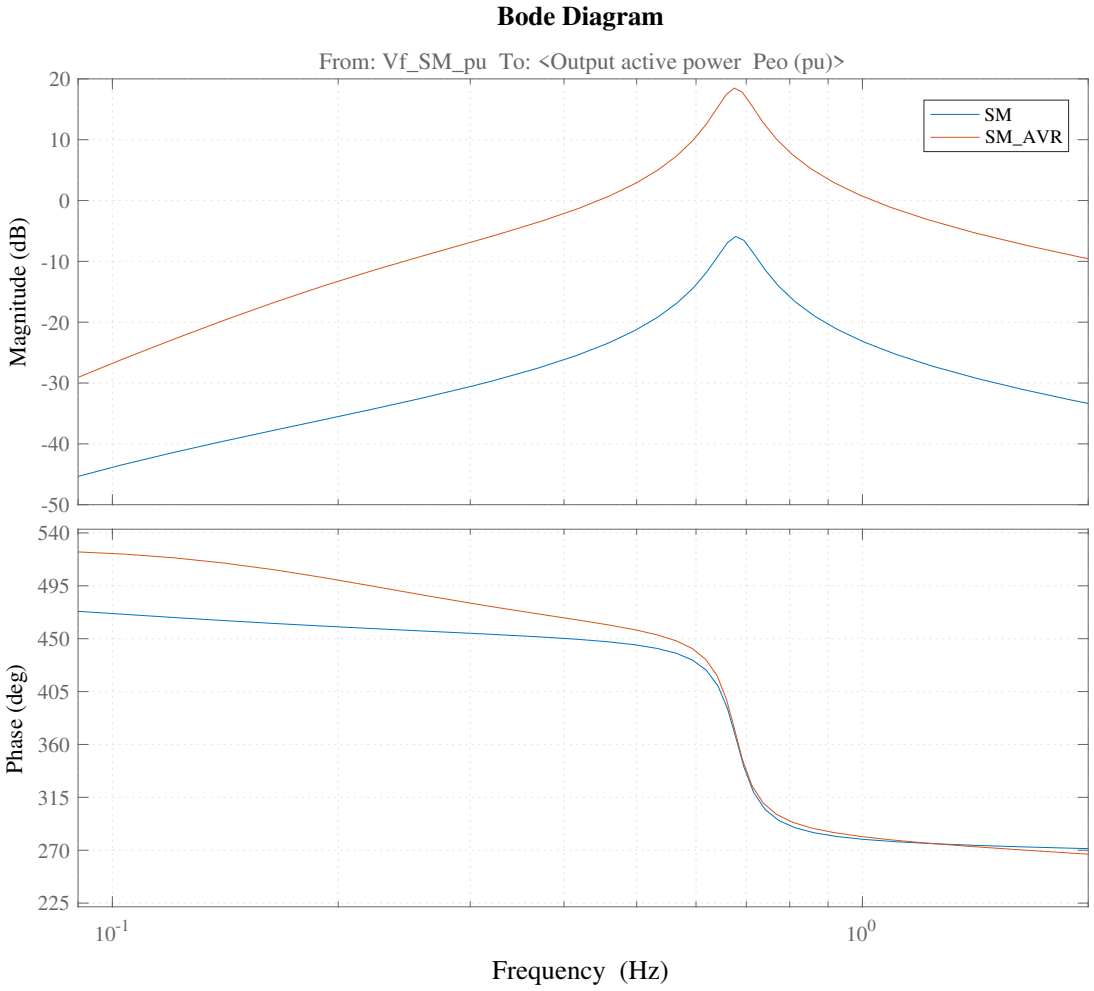

Figure 4.6: Bode plot comparing constant field voltage and AVR reference set as system input of the physical SM.

4.2.3 Interconnection of both Grid Areas

Finally, the two grid areas are interconnected via the emulated PCC, enabling full analysis over both unique dynamics simultaneously. The observations made in Figures 4.3 and 4.4 are tied together with Figure 4.6 by investigating how the inter-area and local oscillations interact with one another, with and without added power oscillation mitigating action.

4.2.3.1 Inter-Area Oscillations without AVR

The frequency response of each machine linearized transfer function from constant field voltage to electrical power output once interconnected is shown in Figure 4.7. Both of their dynamic behavior are familiar, with the exception around the resonance peak of its grid area counterpart. Clearly depicted in the blue curve is an inter-area swing against the emulated SM at 0.43 Hz. The down-shift in phase, followed by an upswing not observed in Figure 4.6 is caused by the oscillatory interaction between the two. Similar occurrence are observed around the local swings of 0.71 Hz when the emulated machine interplay with the power oscillations propagated from the physical machine.

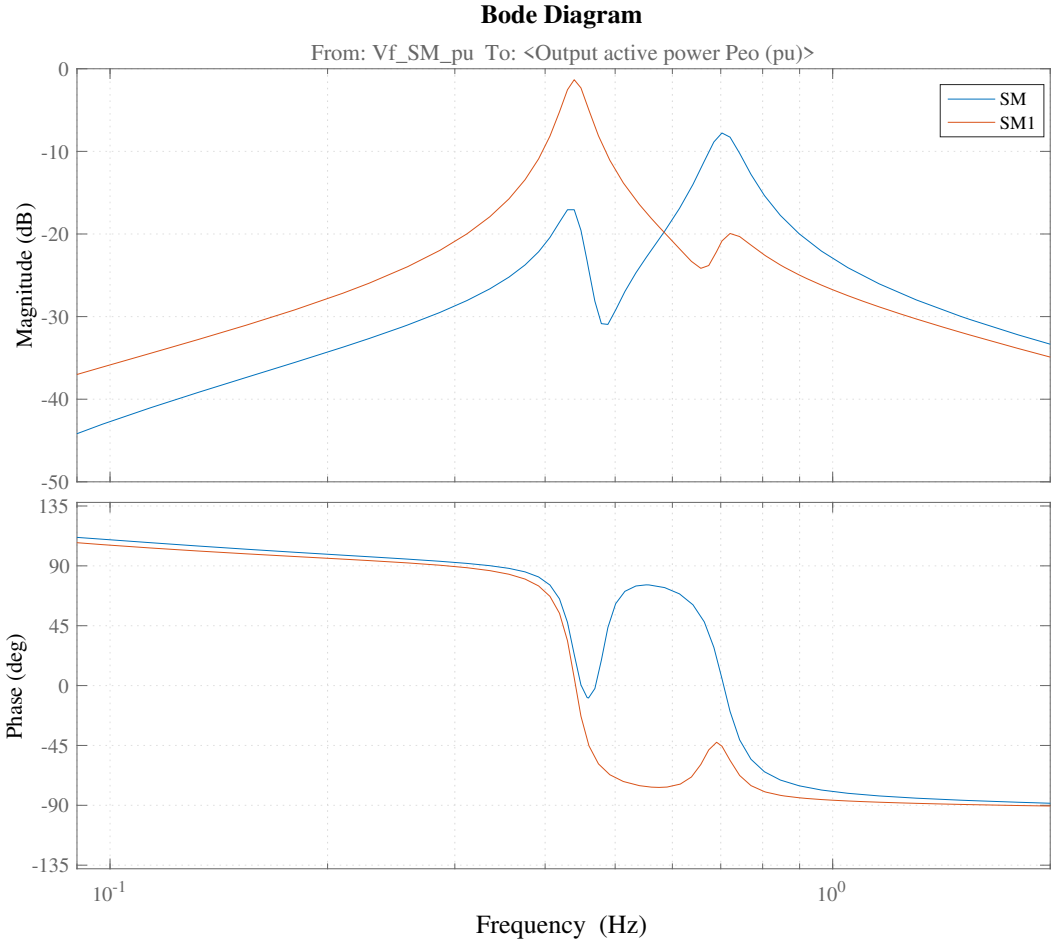

Figure 4.7: Bode plot of power response with both machines interconnected without AVR. Physical SM in blue, emulated SM depicted in red.

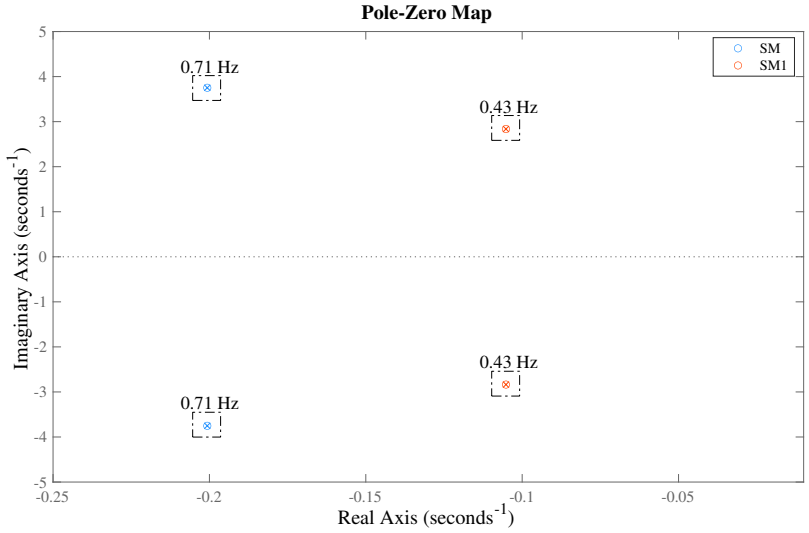

(a) Computed eigenvalues.

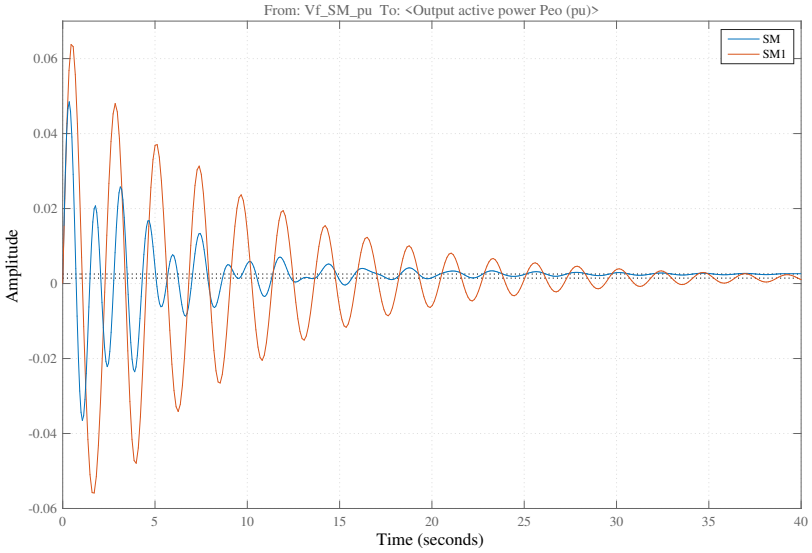

(b) Step response.

Figure 4.8: Linearized simulation results of the two interconnected machines.

The linearized system's eigenvalues are computed and depicted in Figure 4.8a. By inspection, the eigenvalues around the local swings of 0.71 Hz are characterized by a faster but better damped system [6]. The opposite applies for the slower and slightly worse damped inter-area oscillations around 0.43 Hz. Nevertheless, the two system regain stable operation with their eigenvalues being located in the left half-plane.

A step response confirming this is presented in Figure 4.8b. There, it is visually shown how the oscillations of the larger emulated SM decay slower over time, compared to the physical SM. The simulation results also confirm that the smaller physical SM is subjected to inter-area interference from the emulated SM, as illustrated by the bode plot in Figure 4.7.

4.2.3.2 Inter-Area Oscillations with AVR and PSS

With the addition of the exciter and AVR to both SM's, the resonance peak is amplified in magnitude. This was observed in Figure 4.6, becoming more responsive to fast swings. This is discussed extensively in [8]. There it is described as a trade-off between performance of transient stability (higher gain) and robustness in system damping (lower gain) with the AVR. This is visible in Figure 4.9 when both machines are equipped with an AVR. Crucially observed in the bode plot is the secondary resonance peak of the physical SM surpassing the 0 dB limit around the lower inter-area oscillation. This means that the inter-area swings from the emulated grid area impose oscillations on the physical plant, vice versa is seen around the local swings propagated onto the emulated grid area.

Moreover, the damping impact, with the PSS exclusively added to the physical SM is clearly seen in Figure 4.9 where the inter-area resonance peak previously observed around 0.43 Hz on the labs SM is suppressed. Similarly, the local resonance at 0.71 Hz has almost diminished with added system damping. The mitigating action achieved by the PSS on the physical plant alleviate power swings from the emulated grid area, leaving a lesser impactful resonance peak from the larger emulated SM.

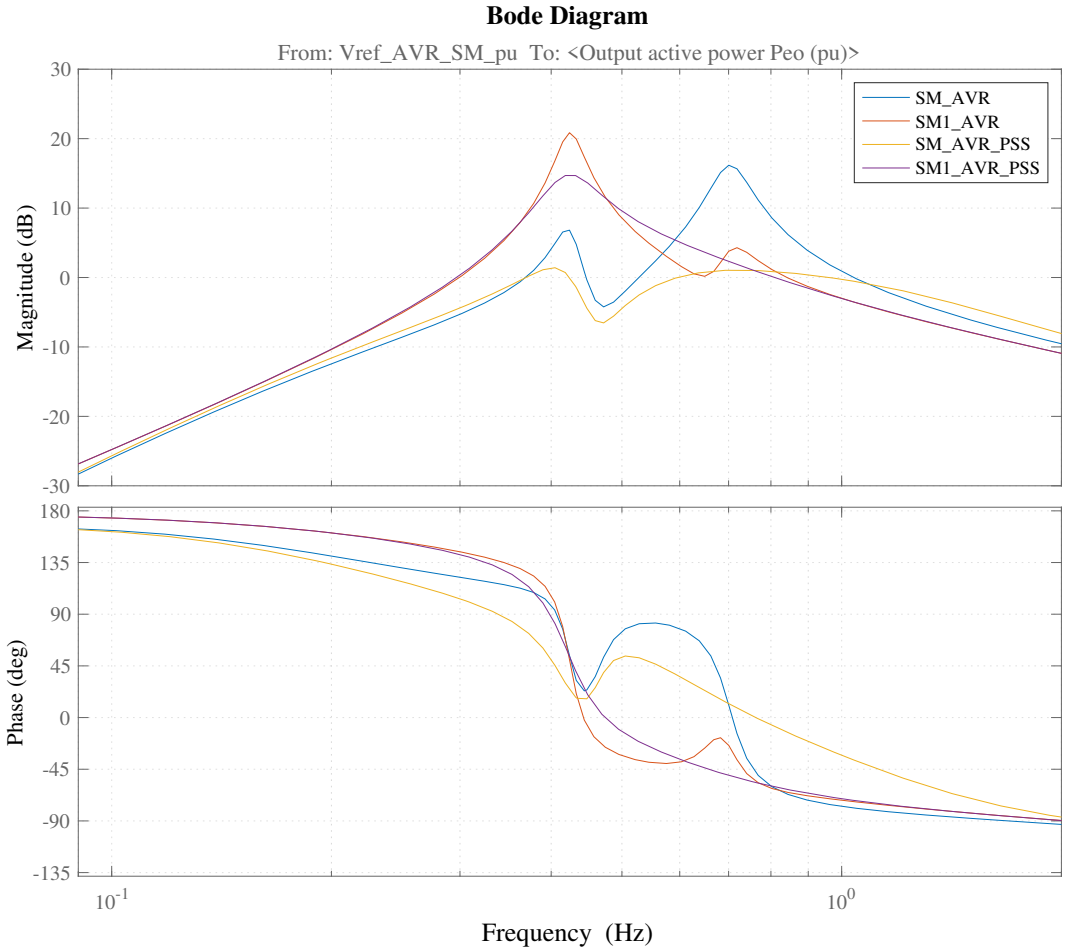

Figure 4.9: Bode plot of both interconnected machines being equipped with AVR, with and without PSS installed on physical SM.

The oscillatory tendencies of both machines with and without PSS added to the physical SM is demonstrated below. The step response of the physical SM in Figure 4.10, with the PSS is considerably better damped, some residual inter-area oscillations are still present since the PSS only partly suppressed the inter-area resonance around 0.43 Hz, as seen by the yellow line in Figure 4.9.

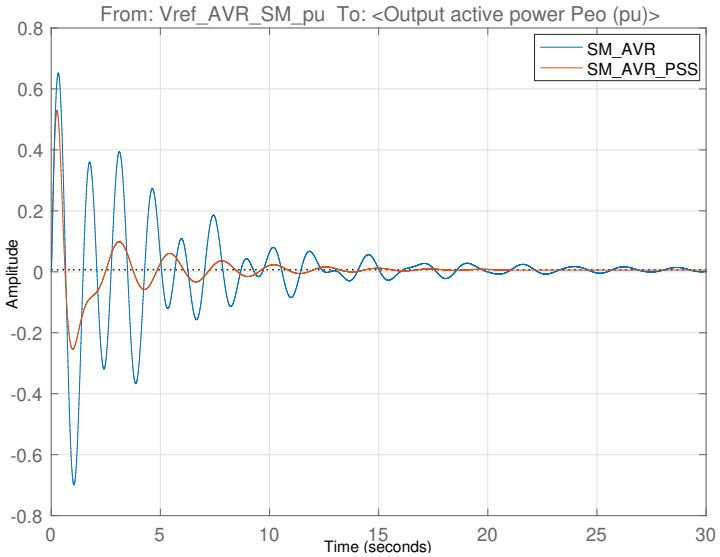

Figure 4.10: Step response of physical SM, with and without PSS.

The over-sized emulated SM also benefits from the added system damping as presented in Figure 4.11, the oscillations observed following the step response with and without the PSS added to the physical SM remain in phase with one another, with significantly lower amplitude. Consequently, the oscillations attenuate faster once the resonance peak of 0.43 Hz reduced in magnitude. This simulation implies that the PSS is enhancing system damping and counteracts inter-area oscillations.

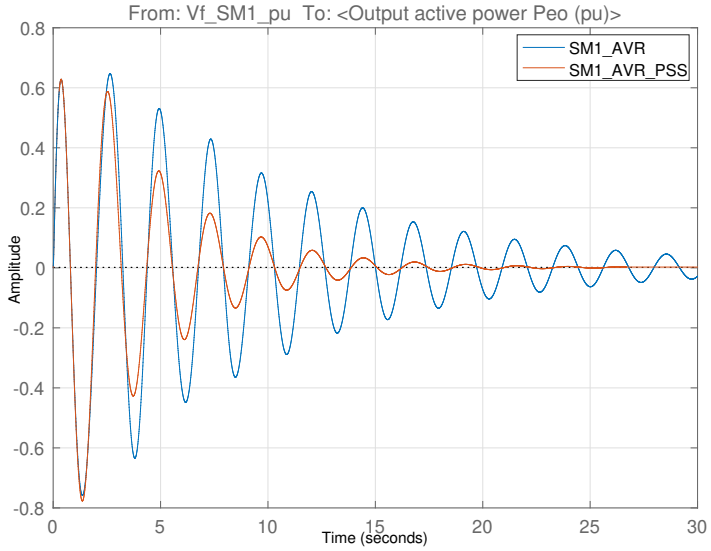

Figure 4.11: Step response of emulated SM, with and without a PSS on the physical SM.

5

Physical Lab Results

The physical lab results in this chapter are presented in two parts. The first part demonstrates the response of the emulated grid when subjected to a disturbance. The second part presents the impact on system damping when implementing the PSS to the physical SM. The two modes of oscillations are then analyzed following the system disturbance from the interconnected emulated grid area.

5.1 Result of Emulated Grid Model Disturbances

The results of the emulated grid model disturbance functionalities described previously in Section 3.3 for the PHIL system are presented here. The outcome and findings following a simulated phase angle jump and variation in voltage magnitude of V_{ref} are evaluated along with their impact on the grid. The emulated SM is interconnected with the emulated PCC through one transmission line section to obtain the distinct resonance peak of 0.43 Hz, while being equipped with the AVR.

5.1.1 Phase Angle Jump Emulated Grid

Initially, the system is running in steady-state mode of operation until a phase angle jump of -20° is applied around 4 s on the emulated grid. Figure 5.1 present the resulting machine frequency, active power, terminal voltage along with field excitation voltage from the excitation system of the emulated SM in blue color. While the PCC active power and voltage is depicted in red color. Following the negative shift in phase, the rotor angle of the emulated SM in relation to the angle reference $\angle V_{ref}$ instantly increases. So does the active power output in the same instant, due to it being strongly coupled with the rotor angle in (2.8). Simultaneously, there is a slight rise in terminal voltage. During this observed rise, the AVR is utilizing the voltage deviation to regulate the excitation field voltage through the PI-regulator. The PCC voltage, characterized by a weaker grid connection point are thus fluctuating more in magnitude, compared with the terminal voltage. Moreover, in Figure 5.1, the inter-area power swings observed at the PCC are displaced opposite to the emulated SM due to their anti-phase angle shift, before both eventually damp out over time. Hence, the instantaneous down-swing in PCC power follows the phase angle jump. Meanwhile, the frequency dynamics gradually swing back and forth, due to the power imbalance according to (2.7). The up-scaled inertia constant prolongs the recovery rate while oscillating at the resonant frequency.

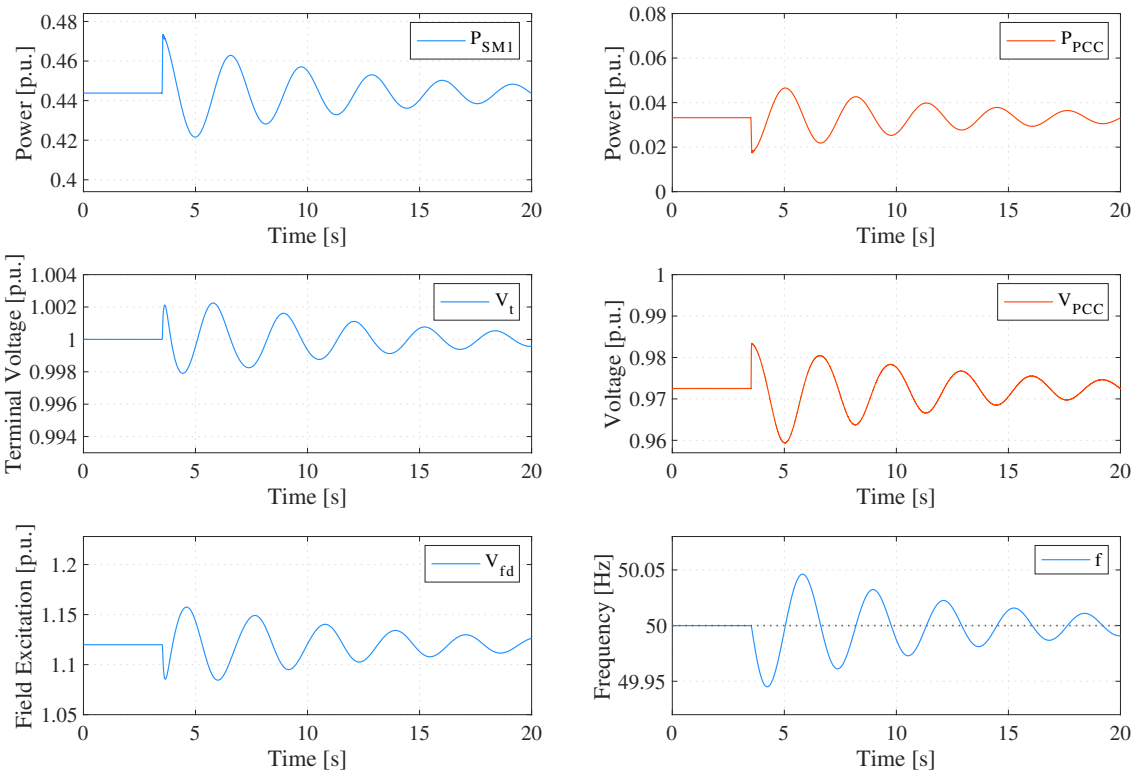

Figure 5.1: Results from the emulated SM and PCC following an instantaneous -20° phase jump from V_{ref}.

5.1.2 Voltage Magnitude Variation Emulated Grid

The system is in steady-state until a voltage dip is applied on the emulated grid, down to 0.8 p.u. temporarily. The decreased voltage magnitude is maintained for 0.3 s before being self-restored back to nominal voltage. The outcome is presented in Figure 5.2, illustrating the behavior of the same system quantities as shown before. During the voltage dip, the field excitation voltage ramps up to regulate the SM's terminal voltage as expected. As a result of the initial voltage drop in the emulated grid, the active power transmitted from the PCC to the emulated grid reduces in the beginning. However, the emulated SM's active power output increases and the frequency reduces in the beginning of the voltage dip, which is unexpected. In fact, the emulated SM's power is expected to drop initially, while the frequency and PCC power should rise from the inter-area interaction.

Moreover, while monitoring the disturbance, the voltage dip is directly reflected in the PCC voltage. The AVR on the emulated SM senses the terminal voltage drop during the voltage depression and operates. Upon self-restoration 0.3 s later, the terminal voltage over-shoots since it takes time for the AVR to regulate down the field current. Consequently, the delayed regulation in voltage magnitude also results in power swings. Thus, by applying a temporary disturbance in the voltage magnitude, power oscillations arise between the emulated SM and PCC.

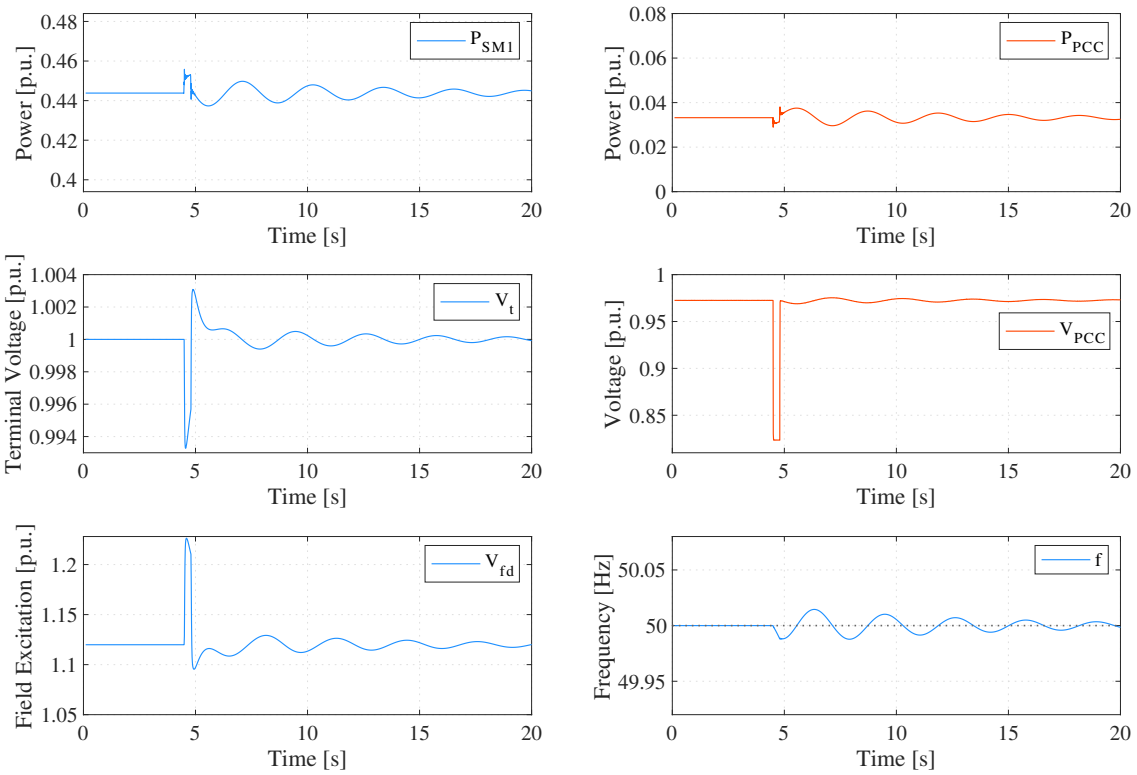

Figure 5.2: Result from the emulated SM and PCC following a temporary 0.8 p.u. voltage drop from V_{ref} lasting 0.3 s.

5.2 PSS Impact on Power System Oscillations

The dynamic interaction of the entire setup illustrated back in Figure 4.1 is examined in the lab environment. The analysis is conducted with and without the PSS installed on the physical lab SM, while being subjected to the 0.43 Hz inter-area oscillation from the emulated grid model. The resulting bode diagram is presented in Figure 5.3, with a frequency spectrum ranging between 0.2-2.0 Hz. Instantly noticeable is the distinct local resonance peak seen at 0.91 Hz, instead of the 0.71 Hz response demonstrated prior during simulations. This is because the active power transmitted from the lab SM to the emulated grid model is about 0.25 p.u., compared to the 0.5 p.u. active power being consumed locally previously in the simulation environment. Thus, increasing the local resonant frequency to 0.91 Hz from (2.19), as the initial operating point of the machine reduces, since the synchronizing power coefficient of the SM increases according to (2.10). Furthermore, the PSS utilizing rotor speed deviation as system input suppresses the occurring local mode peak in Figure 5.3, obtaining the enhanced damping properties on the local mode as demonstrated from the simulations observed in Figure 4.10.

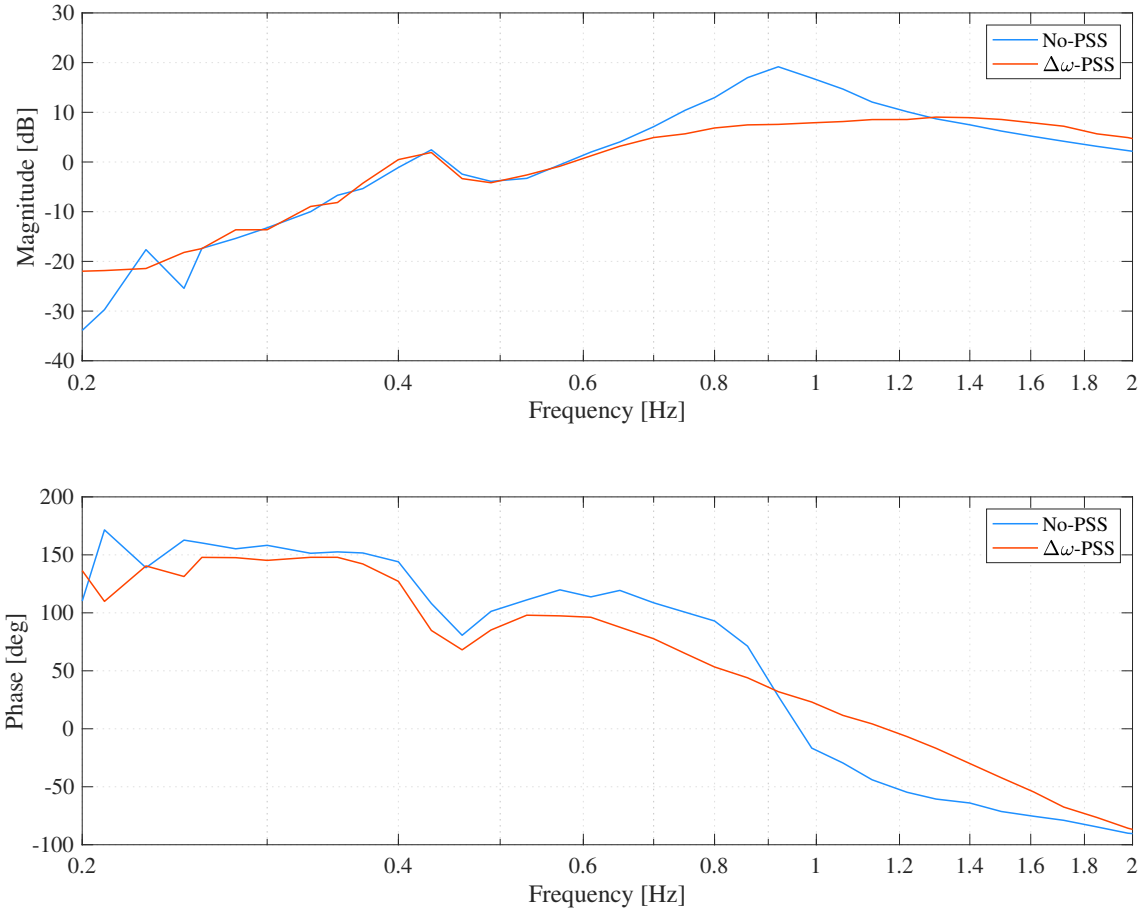

Figure 5.3: Bode plot of physical lab SM being interconnected to the emulated grid model, with and without PSS installed.

This added damping contribution to the physical lab SM is revealed in Figures 5.4 and 5.5, when observing the output active power following a simulated disturbance from the emulated grid model. As demonstrated in the previous section, an instantaneous phase angle jump and voltage drop from V_{ref} displace the power balance following steady-state mode of operation. However seen from the initial swing, the added PSS does not contribute with any synchronizing torque in phase with the rotor angle deviation to enhance transient stability. On the contrary, the damping contribution seen over time is of larger significance.

Consequently, with the PSS, the suppressed local mode resonance of 0.91 Hz observed in Figure 5.3 reduces the oscillatory participation of local power swings by the physical SM. However, the PSS that is utilizing the parameters presented in Appendix A.1 is not able to damp out the inter-area oscillations from the interconnected emulated grid model. As depicted without the PSS in Figure 5.5, the output power contains multiple modes of oscillations following the simulated temporary voltage drop. Thus, making the damping contribution from the added PSS distinguishable for the local mode of oscillation since the oscillations decay considerably faster after the first recurrent power swings.

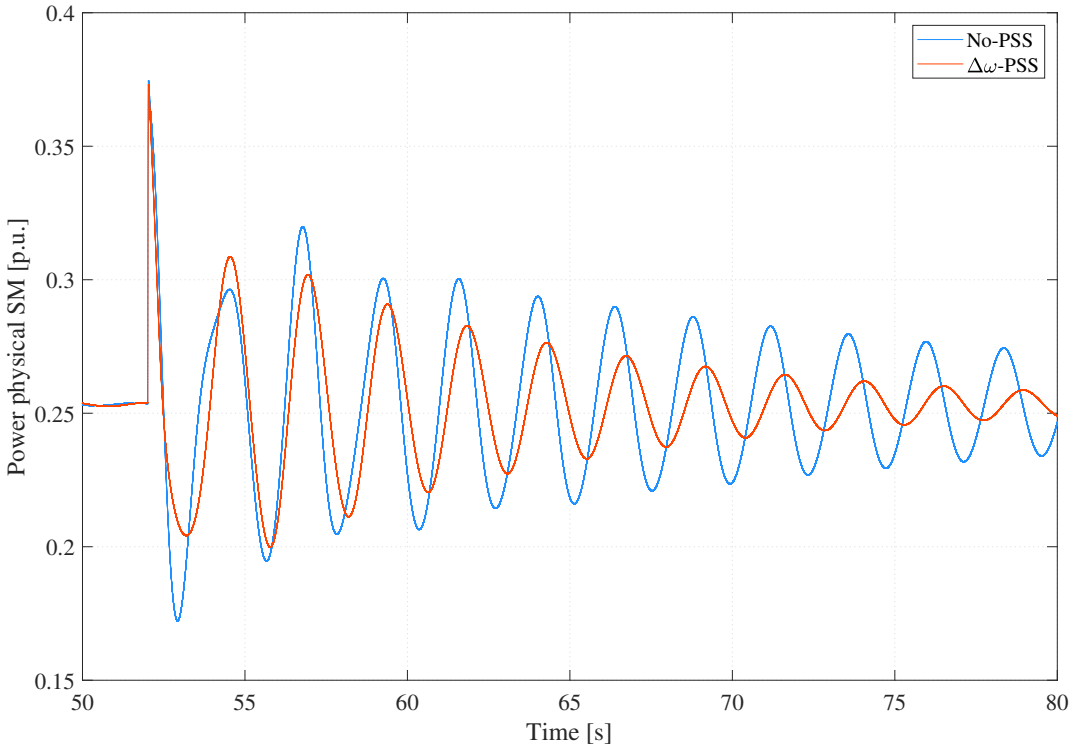

Figure 5.4: Active power of physical 75 kVA lab SM, with and without PSS following an instantaneous -20° phase jump from V_{ref}.

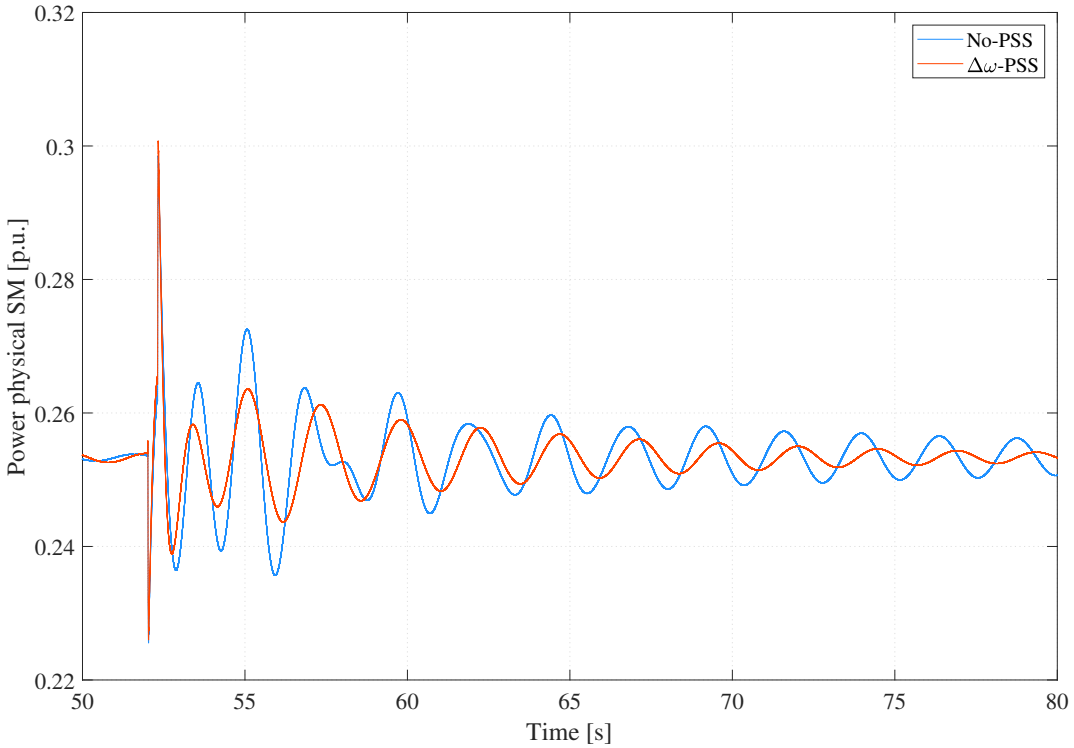

Figure 5.5: Active power of physical 75 kVA lab SM, with and without PSS following a temporary 0.8 p.u. voltage drop from V_{ref} lasting 0.3 s.

6
Conclusion and Future Work

6.1 Conclusion

The thesis work has successfully constructed and designed a PHIL system to emulate a fictitious grid model with real-time varying grid characteristics, interconnected with a physical SM. Through simulations, grid parameters impacting the frequency response were examined to evaluate oscillatory tendencies. In real-time, power oscillations were observed and analyzed in the lab environment. Thus, illustrating the compatibility between a physical and simulated grid area. The grid disturbance is applied in the voltage magnitude and phase angle of the emulated grid, modelled by a controllable voltage source.

The added PSS proved to provide sufficient damping to suppress the local mode resonance peak and thus, enabled enhanced damping to mitigate both simulated disturbances. However, the PSS was not able to damp out the inter-area interference from the emulated grid without tuning it for that specific purpose. Moreover, in the lab environment, the local mode of oscillation was situated within a higher frequency spectrum than anticipated. This resulted from a reduced flow of active power as the initial operating point of the physical lab SM reduced. Similarly, the influence of inter-area oscillations was observed through simulations by varying the emulated SM's inertia time constant, line impedance and also evaluating the characteristics contributed by the AVR. To conclude, the emulated grid model is fully functional to set the right grid conditions and initiate disturbances to observe inter-area oscillations that may occur between the two grid areas.

6.2 Future Work

The following aspects should be considered when further extending the analysis:

- Evaluate different PSS tuning methods to damp inter-area interference from the physical SM's perspective by suppressing the inter-area resonance peak.
- Examine PSS implementation on the emulated SM by intentionally setting incorrect parameter settings, enabling PSS tuning on the physical lab SM to mitigate inter-area interference by the poorly tuned PSS at the emulated SM.
- Integrate renewable energy sources into the emulated grid model together with the emulated SM. Analyzing grid changing characteristics with varying renewable energy penetration levels to evaluate the impact on a future power system.

Bibliography

[1] S. Eftekharnejad, V. Vittal, G. T. Heydt, B. Keel, and J. Loehr, "Small Signal Stability Assessment of Power Systems With Increased Penetration of Photovoltaic Generation: A Case Study," *IEEE Transactions on Sustainable Energy*, vol. 4, no. 4, pp. 960–967, 2013.

[2] J. Quintero, V. Vittal, G. T. Heydt, and H. Zhang, "The Impact of Increased Penetration of Converter Control-Based Generators on Power System Modes of Oscillation," *IEEE Transactions on Power Systems*, vol. 29, no. 5, pp. 2248–2256, 2014.

[3] L. Yu, K. Meng, W. Zhang, J. Dong, and M. Nadarajah, "System Strength Challenges: An Overview of Energy Transition in Australia's National Electricity Market," in *2021 IEEE 4th International Electrical and Energy Conference (CIEEC)*, 2021, pp. 1–6.

[4] R. Stanev and K. Nakov, "Power System Stabilizers for Inverter Dominated Future Power Systems," in *2020 21st International Symposium on Electrical Apparatus Technologies (SIELA)*, 2020, pp. 1–8.

[5] G. Rogers, *Power System Oscillations.*, ser. The Kluwer International Series in Engineering and Computer Science: 539. Kluwer Academic, 2000.

[6] P. Kundur, *Power System Stability and Control*. McGraw-Hill, 1994.

[7] A. Dysko, W. E. Leithead, and J. O'Reilly, "Enhanced Power System Stability by Coordinated PSS Design," *IEEE Transactions on Power Systems*, vol. 25, no. 1, pp. 413–422, 2010.

[8] G. Dudgeon, W. Leithead, A. Dyśko, J. O'Reilly, and J. Mcdonald, "The Effective Role of AVR and PSS in Power Systems: Frequency Response Analysis," *Power Systems, IEEE Transactions on*, vol. 22, pp. 1986 – 1994, 12 2007.

[9] S. Noureen, N. Shamim, V. Roy, and S. Bayne, "Real-Time Digital Simulators: A Comprehensive Study on System Overview, Application, and Importance," *International Journal of Research and Engineering*, vol. 4, pp. 266–277, 12 2017.

[10] J. Bélanger, P. Venne, and J.-N. Paquin, "The What, Where, and Why of Real-Time Simulation," *Planet RT*, pp. 37–49, 01 2010.

[11] UN, "Transforming our world: The 2030 Agenda for Sustainable Development," *A/RES/70/1*, October 2015.

[12] IEA, *Tracking SDG 7: The Energy Progress Report (2021)*. World Bank, June, 2021.

[13] P. Kundur, J. Paserba, V. Ajjarapu, G. Andersson, A. Bose, C. Canizares, N. Hatziargyriou, D. Hill, A. Stankovic, C. Taylor, T. Van Cutsem, and V. Vittal, "Definition and Classification of Power System Stability IEEE/CIGRE

Joint Task Force on Stability Terms and Definitions," *IEEE Transactions on Power Systems*, vol. 19, no. 3, pp. 1387–1401, 2004.

[14] J. Machowski, J. W. Bialek, and J. R. Bumby, *Power System Dynamics: Stability and Control.* Oxford: John Wiley, October 2008.

[15] H. Saadat, *Power System Analysis.* McGraw-Hill, 2009.

[16] M. Gibbard, P. Pourbeik, and D. Vowles, *Small-Signal Stability, Control and Dynamic Performance of Power Systems.* University of Adelaide Press, 2015. [Online]. Available: http://www.jstor.org/stable/10.20851/j.ctt1sq5wzz

[17] T. Glad and L. Ljung, *Control Theory.* CRC press; 1st ed., 2000.

[18] V. Jerkovic Stil, K. Miklosevic, and Z. Spoljaric, "Excitation System Models of Synchronous Generator," 09 2018.

[19] L. Harnefors, M. Hinkkanen, O. Wallmark, and A. G. Yepes, "Control of Voltage-Source Converters and Variable-Speed Drives," Compendium.

[20] K. Prasertwong, N. Mithulananthan, and D. Thakur, "Understanding Low-Frequency Oscillation in Power Systems," *The International Journal of Electrical Engineering & Education*, vol. 47, no. 3, pp. 248–262, 2010. [Online]. Available: https://doi.org/10.7227/IJEEE.47.3.2

[21] N. Nikolaev, K. Dimitrov, and Y. Rangelov, "A Comprehensive Review of Small-Signal Stability and Power Oscillation Damping through Photovoltaic Inverters," *Energies*, vol. 14, no. 21, 2021. [Online]. Available: https://www.mdpi.com/1996-1073/14/21/7372

[22] A. A. Ba-muqabel and M. A. Abido, "Review of Conventional Power System Stabilizer Design Methods," in *2006 IEEE GCC Conference (GCC)*, 2006, pp. 1–7.

[23] "IEEE Recommended Practice for Excitation System Models for Power System Stability Studies," *IEEE Std 421.5-2016 (Revision of IEEE Std 421.5-2005)*, pp. 1–207, 2016.

[24] ENTSO-E, "Analysis of CE Inter-Area Oscillations of 1st December 2016," *ENTSO-E: Brussels, Belgium*, 2017.

[25] R. Xie, I. Kamwa, D. Rimorov, and A. Moeini, "Fundamental study of common mode small-signal frequency oscillations in power systems," *International Journal of Electrical Power and Energy Systems*, vol. 106, pp. 201–209, 2019. [Online]. Available: https://www.sciencedirect.com/science/article/pii/S0142061518319513

[26] K.-S. Shim, S.-J. Ahn, and J.-H. Choi, "Synchronization of Low-Frequency Oscillation in Power Systems," *Energies*, vol. 10, no. 4, 2017. [Online]. Available: https://www.mdpi.com/1996-1073/10/4/558

[27] M. Klein, G. Rogers, and P. Kundur, "A Fundamental Study of Inter-Area Oscillations in Power Systems," *IEEE Transactions on Power Systems*, vol. 6, no. 3, pp. 914–921, 1991.

[28] Regatron, "Technical Datasheets," www.regatron.com/product/overview/programmable-bidirectional-ac-power-sources/tc-acs-series/#technical-datasheets, 2021, Accessed: 2021-12-20.

[29] M. Gustafsson and N. Krantz, *Voltage Collapse in Power Systems: Analysis of Component Related Phenomena Using a Power System Model*, ser. Technical

report / School of Electrical and Computer Engineering, Chalmers University of Technology. L: 215, 1995.

[30] C. L. Fortescue, "Method of Symmetrical Co-Ordinates Applied to the Solution of Polyphase Networks," *Transactions of the American Institute of Electrical Engineers*, vol. XXXVII, no. 2, pp. 1027–1140, 1918.

[31] dSPACE GmbH, "MicroLabBox, Compact Power in the Lab," https://www.dspace.com/en/pub/home/products/hw/microlabbox.cfm, 2015, Accessed: 2022-03-01.

[32] ——, "ControlDesk, Brochure 2021," https://www.dspace.com/en/inc/home/products/sw/experimentandvisualization/controldesk.cfm, 2021, Accessed: 2022-04-25.

[33] E. Clarke, *Circuit Analysis of A-C Power Systems*, ser. General Electric series, 1950.

[34] Y. Qian, X. Yuan, and M. Zhao, "Analysis of Voltage Control Interactions and Dynamic Voltage Stability in Multiple Wind Farms," in *2016 IEEE Power and Energy Society General Meeting (PESGM)*, 2016, pp. 1–5.

[35] MathWorks, "Simscape Electrical Reference (Specialized Power Systems) R2021b," 2021, Accessed: 2022-03-02.

[36] A. Moeini, I. Kamwa, P. Brunelle, and G. Sybille, "Synchronous Machine Stability Model, an Update to IEEE Std 1110-2002 Data Translation Technique," in *2018 IEEE Power Energy Society General Meeting (PESGM)*, 2018, pp. 1–5.

[37] S. Chapman, *Electric Machinery Fundamentals*. McGraw-Hill Education, 2011.

[38] MathWorks, "Simulink Control Design User's Guide R2022a," 2022, Accessed: 2022-04-07.

A

Appendix 1

The PSS2B model used thought this thesis work is presented here along with the parameters implemented [23].

A.1 PSS2B Model Parameters

With the PSS2B model, the simplified diagram shown back in Figure 2.9 is extended, consisting of two washout high-pass filters and three lead-lag filters for phase compensation. Thus, the equivalent transfer function becomes

$$G_{PSS}(s) = K_{PSS}\frac{sT_{w1}}{1+sT_{w1}}\frac{sT_{w2}}{1+sT_{w2}}\frac{1+sT_1}{1+sT_2}\frac{1+sT_3}{1+sT_4}\frac{1+sT_{10}}{1+sT_{11}} \tag{A.1}$$

with the gain K_{PSS} set to a value of 6.

Furthermore the output limiter is set ± 0.05 p.u., for its upper and lower limits respectively. Table A.1 presents the time constants values implemented for the filters in (A.1).

Table A.1: PSS2B time constant parameter values.

Parameter	Value [s]
T_{w1}	5.0
T_{w2}	5.0
T_1	0.5
T_2	0.2
T_3	0.5
T_4	0.2
T_{10}	0.5
T_{11}	0.2

DEPARTMENT OF ELECTRICAL ENGINEERING
CHALMERS UNIVERSITY OF TECHNOLOGY
Gothenburg, Sweden
www.chalmers.se

CHALMERS
UNIVERSITY OF TECHNOLOGY